NAVAL POSTGRADUATE SCHOOL

MONTEREY, CALIFORNIA

THESIS

NOVEL NATURAL CONVECTION HEAT SINK DESIGN CONCEPTS FROM FIRST PRINCIPLES

by

Derek E. Fletcher

June 2016

Thesis Advisor: Garth Hobson
Second Reader: Joshua Gordis

Approved for public release; distribution is unlimited

THIS PAGE INTENTIONALLY LEFT BLANK

REPORT DOCUMENTATION PAGE			*Form Approved OMB No. 0704–0188*
Public reporting burden for this collection of information is estimated to average 1 hour per response, including the time for reviewing instruction, searching existing data sources, gathering and maintaining the data needed, and completing and reviewing the collection of information. Send comments regarding this burden estimate or any other aspect of this collection of information, including suggestions for reducing this burden, to Washington headquarters Services, Directorate for Information Operations and Reports, 1215 Jefferson Davis Highway, Suite 1204, Arlington, VA 22202-4302, and to the Office of Management and Budget, Paperwork Reduction Project (0704-0188) Washington, DC 20503.			
1. AGENCY USE ONLY ***(Leave blank)***	**2. REPORT DATE** June 2016	**3. REPORT TYPE AND DATES COVERED** Master's Thesis	
4. TITLE AND SUBTITLE NOVEL NATURAL CONVECTION HEAT SINK DESIGN CONCEPTS FROM FIRST PRINCIPLES		**5. FUNDING NUMBERS**	
6. AUTHOR(S) Derek E. Fletcher			
7. PERFORMING ORGANIZATION NAME(S) AND ADDRESS(ES) Naval Postgraduate School Monterey, CA 93943-5000		**8. PERFORMING ORGANIZATION REPORT NUMBER**	
9. SPONSORING /MONITORING AGENCY NAME(S) AND ADDRESS(ES) Project supported by the Office of Naval Research's (ONR) Energy Systems Technical Evaluation Program (ESTEP), supported by Dr. Richard Carlin and under the technical monitoring of Stacey Curtis.		**10. SPONSORING / MONITORING AGENCY REPORT NUMBER**	
11. SUPPLEMENTARY NOTES The views expressed in this thesis are those of the author and do not reflect the official policy or position of the Department of Defense or the U.S. Government. IRB Protocol number ____N/A____.			
12a. DISTRIBUTION / AVAILABILITY STATEMENT Approved for public release; distribution is unlimited		**12b. DISTRIBUTION CODE**	

13. ABSTRACT (maximum 200 words)

This was a two-part numerical study using ANSYS Fluent to develop novel heat sink concepts from first principles. The objective of this research was to highlight geometric structures that incorporate the principles of the stack effect to improve the heat transfer capability of a heat sink under natural convection. The first part investigated the heat transfer/fluid flow characteristics of vertically aligned tubes. The gaps between tubes break up the thermal and velocity boundary layers and the moving fluid within a tube entrains the cooler ambient air surrounding the gap, thus increasing mass flow rate and average Nusselt number through each tube. The optimal gap-to-length ratio varies depending on the number of tubes in the system. The second part built upon the insight gained to develop heat sinks to compare to pin-fin heat sinks. A tube system heat sink provides a significant improvement in the heat transfer capability over a circular pin-fin arrangement, demonstrated by an increase in both the overall heat transferred and average heat transfer coefficient. The principles discussed in this study have the potential to expand the capability of natural convective heat transfer.

14. SUBJECT TERMS natural convection, free convection, passive cooling, heat sink, tube system, pin-fin, hollow pin-fin, heat sink design			**15. NUMBER OF PAGES** 67
			16. PRICE CODE
17. SECURITY CLASSIFICATION OF REPORT Unclassified	**18. SECURITY CLASSIFICATION OF THIS PAGE** Unclassified	**19. SECURITY CLASSIFICATION OF ABSTRACT** Unclassified	**20. LIMITATION OF ABSTRACT** UU

NSN 7540–01-280-5500 Standard Form 298 (Rev. 2–89)
Prescribed by ANSI Std. 239–18

THIS PAGE INTENTIONALLY LEFT BLANK

Approved for public release; distribution is unlimited

NOVEL NATURAL CONVECTION HEAT SINK DESIGN CONCEPTS FROM FIRST PRINCIPLES

Derek E. Fletcher
Lieutenant Commander, United States Navy
B.S., Southwestern University, 2005
M.E.M., Old Dominion University, 2012

Submitted in partial fulfillment of the
requirements for the degree of

MASTER OF SCIENCE IN MECHANICAL ENGINEERING

from the

NAVAL POSTGRADUATE SCHOOL
June 2016

Approved by: Garth Hobson
Thesis Advisor

Joshua Gordis
Second Reader

Garth Hobson
Chair, Department of Mechanical and Aerospace Engineering

THIS PAGE INTENTIONALLY LEFT BLANK

ABSTRACT

This was a two-part numerical study using ANSYS Fluent to develop novel heat sink concepts from first principles. The objective of this research was to highlight geometric structures that incorporate the principles of the stack effect to improve the heat transfer capability of a heat sink under natural convection. The first part investigated the heat transfer/fluid flow characteristics of vertically aligned tubes. The gaps between tubes break up the thermal and velocity boundary layers and the moving fluid within a tube entrains the cooler ambient air surrounding the gap, thus increasing mass flow rate and average Nusselt number through each tube. The optimal gap-to-length ratio varies depending on the number of tubes in the system. The second part built upon the insight gained to develop heat sinks to compare to pin-fin heat sinks. A tube system heat sink provides a significant improvement in the heat transfer capability over a circular pin-fin arrangement, demonstrated by an increase in both the overall heat transferred and average heat transfer coefficient. The principles discussed in this study have the potential to expand the capability of natural convective heat transfer.

THIS PAGE INTENTIONALLY LEFT BLANK

TABLE OF CONTENTS

THIS PAGE INTENTIONALLY LEFT BLANK

LIST OF FIGURES

LIST OF TABLES

THIS PAGE INTENTIONALLY LEFT BLANK

LIST OF ACRONYMS AND ABBREVIATIONS

A	area
C	skin friction coefficient
c	specific heat
D	tube diameter
f	friction factor
$\vec{g}$	gravity vector
G	gap length between vertical tubes
Gz	Graetz number
$\overline{h}$	average heat transfer coefficient
k	thermal conductivity
L	tube length
$\dot{m}$	mass flow rate
$\overline{Nu_D}$	average Nusselt number
p	pressure
Pr	Prandtl number
q''	heat flux
Q	heat transfer
R	resistance
Re_D	Reynolds number
St	Stanton number
T	temperature
ΔT_{lm}	log-mean temperature difference
$\vec{u}$	velocity vector
u	fluid velocity
ρ	fluid density
μ	dynamic viscosity
ε	emissivity

σ Stefan-Boltzmann constant

τ shear stress

LIST OF SUBSCRIPTS

$conv$	convection
cs	cross-section
D	diameter
e	entrance
eff	effective
f	fluid
m,i	mean mixing-cup at inlet
m,o	mean mixing-cup at outlet
$open$	open boundary
p	pressure
rad	radiation
s	surface
th	thermal
tot	total
$tube$	tube
x	local position
∞	ambient

THIS PAGE INTENTIONALLY LEFT BLANK

ACKNOWLEDGMENTS

First, I must express my very profound gratitude to my wife, Kristina, and my children, Kacie, Colton, and Caleb, whose love and support have been the greatest joy in my life. Thank you to my parents and sister, who have taught me the value of hard work and laid the building blocks of the man that I have grown into.

I would like to acknowledge my advisor, Dr. Garth Hobson, and second reader, Dr. Joshua Gordis, both of the Department of Mechanical and Aerospace Engineering at Naval Postgraduate School. I am grateful for their comments and valuable insight for this thesis. Many thanks to my mentor, Dr. Sanjeev Sathe, who has taught me much more than can ever be expressed.

"For the Lord gives wisdom; from his mouth come knowledge and understanding." —Proverbs 2:6

THIS PAGE INTENTIONALLY LEFT BLANK

I. INTRODUCTION

This thesis conducted a two-part, detailed numerical study that analyzed geometric structures that have the potential to increase the overall heat transfer capability of a heat sink when incorporated into the design. The first part of the study explored the possibility of increasing the mass flow rate and overall heat transfer capability through vertical tubes by utilizing principles of the stack effect (i.e., using multiple inlets to create a suction effect to draw cooler ambient air into the tube). The second part of the study used the insight gained to develop novel heat sinks and compare them to standard pin-fin heat sinks. Three-dimensional computations of flow and heat transfer were carried out for constant temperature heat addition for single vertical tubes, multiple stacked tubes, tube system heat sinks and circular pin-fin heat sinks.

A. NATURAL CONVECTION

Natural convection heat transfer has been studied quite extensively due to its many applications and high reliability. In natural convection, fluid motion is induced due to density variations caused by a temperature gradient in the working fluid that is subjected to a body force (e.g., gravity). Elenbaas [1] thoroughly explored the free convective heat transfer from the inner surface of vertical tubes of different cross-sections such as equilateral triangle, square, rectangle, and circle. More recently, Totala et al. [2] experimentally verified that the local heat transfer coefficient is a maximum at the entrance to a vertical tube subjected to free convective heat transfer and subsequently decreases as the thermal boundary layer grows. Davis and Perona [3] concluded that the development entrance length for free convection flows in vertical tubes is quite large and the assumption of fully developed flow is invalid for many cases. Due to the work of Davis and Perona, it is imperative to understand the entrance region to fully grasp the heat transfer capability of vertical tubes subjected to natural convection. Sieder and Tate [4] developed a correlation, eqn. (1.1), for the average Nusselt $\left(\overline{Nu_D}\right)$ number and the Graetz $\left(Gz\right)$ number for the combined entry length for internal laminar flow. The

combined entry length means that both the thermal and velocity boundary layers are developing at the same time.

$$\overline{Nu_D} = 1.86\left(Gz\right)^{1/3}\left(\frac{\mu}{\mu_s}\right)^{0.14} \qquad (1.1)$$

$$0.60 \le \mathrm{Pr} \le 5$$

$$0.0044 \le \left(\frac{\mu}{\mu_s}\right) \le 9.75$$

$$\overline{Nu_D} \ge 3.66$$

In addition to Sieder and Tate, Incropera [5] discusses a correlation developed by Hausen, eqn. (1.2), for the thermal entry length for moderate Prandtl (Pr) numbers, which can also be used for a combined entry length with high Pr fluids. Gnielinski [6] developed a $\overline{Nu_D}$ vs Gz correlation, eqn. (1.3), for fully developed turbulent flows. All three of these correlations are discussed by Incropera et al. [5].

$$\overline{Nu_D} = 3.66 + \frac{0.0668\left(D/L\right)\mathrm{Re}_D\,\mathrm{Pr}}{1+0.04\left[\left(D/L\right)\mathrm{Re}_D\,\mathrm{Pr}\right]^{2/3}} \qquad (1.2)$$

$$\overline{Nu_D} = \frac{\left(f/8\right)\left(\mathrm{Re}_D - 1000\right)\mathrm{Pr}}{1+12.7\left(f/8\right)^{1/2}\left(\mathrm{Pr}^{2/3}-1\right)} \qquad (1.3)$$

B. HEAT TRANSFER CAPABILITY

When improving the convective heat transfer capability from a surface there are three possible avenues: increase the temperature difference, increase the heat transfer surface area, or increase the heat transfer coefficient. The most widely used method is to increase the surface area by the addition of fins. Different designs, concentrations, and orientations of these fins have been analyzed in numerous experimental and numerical studies.

The alignment of pin-fins, either staggered or inline, was shown to affect the heat transfer performance in natural convection with the conclusion that inline pin-fins yield a

higher heat transfer rate than staggered [7]. The studies conducted by Sertkay et al. and Huang et al. both indicate that depending on the design, pin-fins in the horizontal and upward vertical direction can be comparable while the downward vertical direction provides the worst heat transfer characteristics [8,9].

During the literature review, only two studies were uncovered that analyzed hollow pin-fins. Elshafei [10] compared a hollow pin-fin to solid pin-fins subjected to natural convection under different orientations and concluded that heat transfer performance for hollow pin-fins was better than that of solid fins, which resulted in a lower temperature difference between the base plate and the ambient air for a given heat input. Awad [11], on the other hand, compared straight fins, solid pin-fins, hollow pin-fins, and convergent-divergent fins and concluded hollow pin-fins have the lowest heat transfer performance, based on having the lowest average heat flux. In both of these studies, the hollow pin-fins had one entry point at the base of the pin-fin. At first glance, these two articles appear to contradict each other; however, this study offers an explanation as to how both are correct based on their respective experimental setup.

C. NATURAL VENTILATION

For large-scale applications, natural convection is utilized to ventilate buildings. There are three general techniques for natural ventilation depicted in Figure 1. Namely: 1) single-sided ventilation, 2) wind-pressure driven cross-ventilation, and 3) buoyancy pressure-driven stack (chimney) ventilation [12].

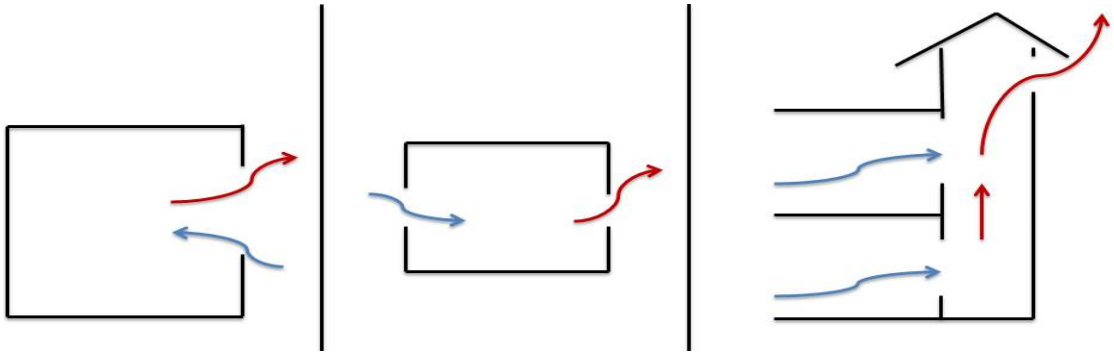

Figure 1. Single-Sided Ventilation (Left); Wind-Pressure Driven Cross-Ventilation (Middle); Buoyancy Pressure-Driven Stack Ventilation (Right)

In stack ventilation single or multiple chimneys are designed with various air inlets to remove the hotter internal air creating a suction effect that draws in cooler fresh air. There are many factors that influence the performance of stack ventilation, which includes the size and location of the air inlets and openings. Krzaczek et al. concluded that the stack effect could be generated with a temperature difference as little as 12 degrees Celsius [12].

II. NUMERICAL MODEL AND DATA REDUCTION

The computational fluid dynamics software utilized for all models discussed in this study was ANSYS FLUENT. At the basic level, the problem considered for numerical modeling was a vertical tube under natural convection conditions subjected to constant temperature heat addition. Many additional geometries were created with multiple tubes stacked vertically with a gap between each tube; Figure 2 represents the basic geometries analyzed. The left tube model depicts a single tube with a length-to-diameter ratio equal to five and the right graphic depicts a multiple stacked tube model with a length-to-diameter ratio equal to one and a gap-to-length ratio equal to 0.4. In the multiple stacked tube models the opening is a gap between the heated tube segments.

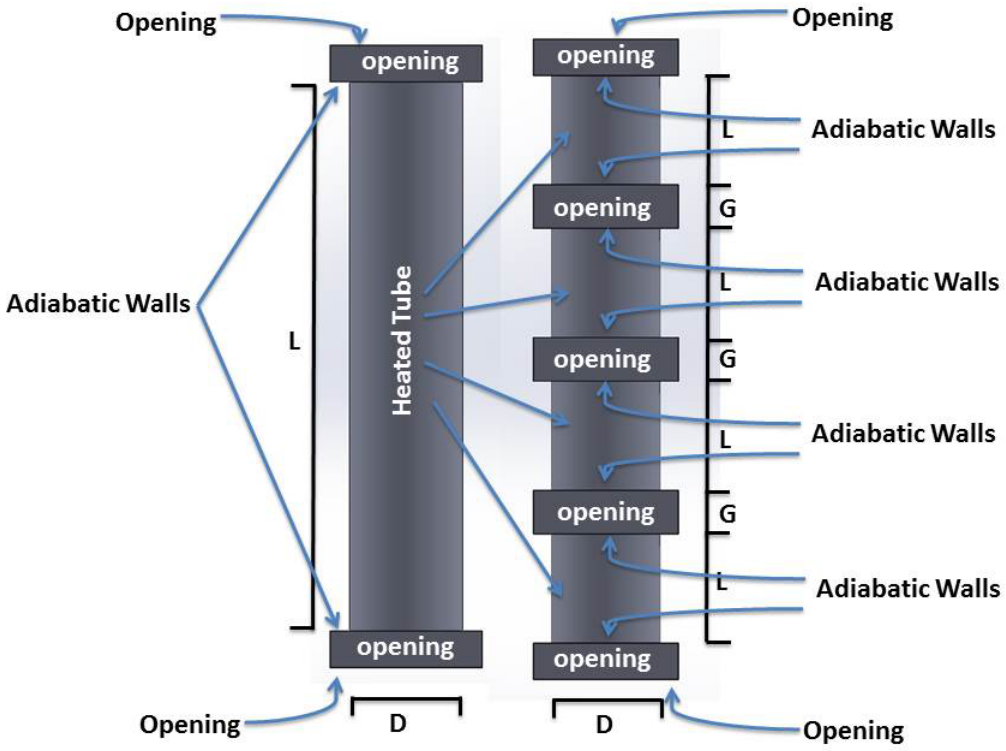

Figure 2. Representation of Basic Geometries Created for Initial Analysis

In all geometries, only the fluid domain was analyzed, which simplified the model by not using a fluid-solid interface and neglected conduction through the heat sink. Figure 3 depicts the heat sink designs analyzed.

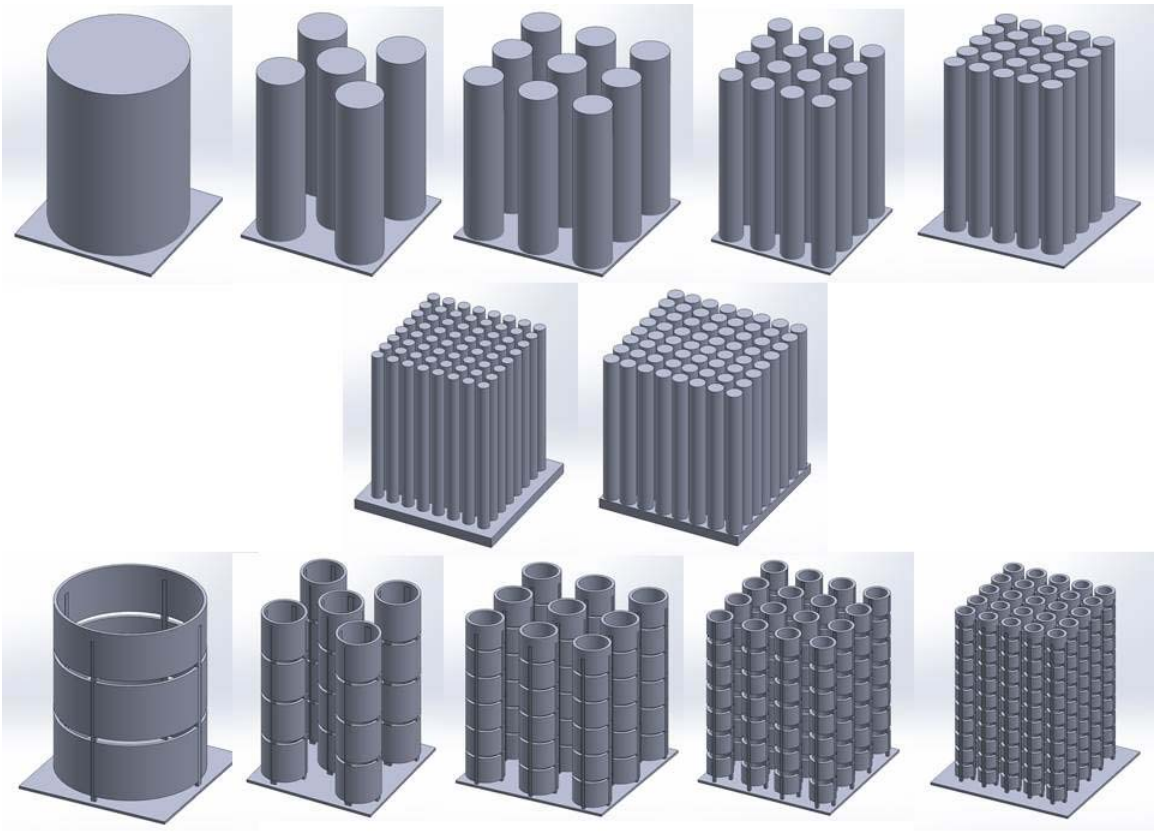

Figure 3. Heat Sink Designs Analyzed

A. MODEL ASSUMPTIONS

For the single tube and multiple stacked tube geometries, the vertical tubes were assigned to be smooth walled, with a no-slip boundary condition, and maintained at a constant temperature. On top of and below each tube was a box that contained open boundaries with a zero Pascal relative pressure across the boundary with an ambient temperature below the tube wall temperature. The horizontal sections directly connected to the tubes were assumed adiabatic, smooth walls with a no-slip boundary condition as shown in Figure 2.

The heat sink surfaces were assigned to be smooth walled, with a no-slip boundary condition, and maintained at a constant temperature. The open boundaries were the four walls and top of the fluid space with a zero Pascal relative pressure across the boundary and an ambient temperature below the tube wall temperature.

All numerical models were solved using the Boussinesq buoyancy approximation. Additional assumptions made in the numerical model include:

- Fluid flow is steady state, laminar, and incompressible.
- Thermodynamic-physical properties of the fluid are independent of temperature.
- Viscous dissipation and pressure stress terms are negligible.
- Thermal radiation effects are neglected.

B. GOVERNING EQUATIONS

Based on the previously described assumptions, the governing equations for steady fluid motion are:

$$Continuity: \nabla \bullet \vec{u} = 0 \tag{2.1}$$

$$Momentum: \rho_\infty \left(\vec{u} \bullet \nabla \vec{u}\right) = -\nabla p + \mu \nabla^2 \vec{u} + \rho_\infty \vec{g} \left(\frac{T - T_\infty}{T_\infty}\right) \tag{2.2}$$

$$Energy: \rho_\infty c_p \left(\nabla \bullet \vec{u} T\right) = k_f \nabla^2 T \tag{2.3}$$

Where the third term on the right hand side of eqn. 2.2 is the buoyancy force from the Boussinesq approximation.

C. NUMERICAL PROCEDURE

The governing equations were solved using the finite volume method. The discretized equations were solved using a pressure-based solver via the SIMPLE algorithm. Information on the pressure-based solver utilized by ANSYS FLUENT can be found in the ANSYS Fluent Theory Guide and the SIMPLE algorithm is discussed by Patankar [13,14]. For the single tube and multiple stacked tube geometries, the mesh size was refined until there was no significant change in the results from one mesh size to the

more refined size. The residuals were driven to less than 1E-6 and convergence was assumed when the residuals showed negligible change over 100 iterations. For the heat sinks, a fine mesh size was used in the ANSYS meshing tool and convergence was assumed when the energy residual showed negligible change over 100 iterations. Further refinement of this mesh size was not conducted based on the observations while analyzing single tube and multiple stacked tube geometries. From that analysis it was determined that the energy residuals will converge with a less refined mesh than the velocity residuals. It was noted that flow patterns did not change with a refinement of the mesh. The change was in the velocity of the fluid, which was accompanied with an equivalent change in the temperature difference, resulting in a negligible change in the overall heat transfer. Various ANSYS mesh and physics reports are included in Appendix A.

Since the only heat addition into the system was via the heated tube walls, the overall energy balance was calculated as follows:

$$Energy\ Balance(\%) = \frac{Energy_{out} - Energy_{in}}{Energy_{in}} * 100 = \frac{\left(A_s q''\right)_{open} - \left(A_s q''\right)_{tube}}{\left(A_s q''\right)_{tube}} * 100 \tag{2.4}$$

The average energy balance for the single tube and multiple stacked tubes was 0.0027% and the energy balance in the worst case was 0.011%. While the average energy balance for the heat sinks was 0.11% and 1.72% in the worst case.

A heat transfer check was calculated for the single tube and multiple stacked tube models by comparing the heat transfer calculated from the total heat generated to the summation of the heat transfer from each individual tube as follows:

$$Heat\ Transfer\ Check(\%) = \frac{\left(A_s q''\right)_{tube} - \sum \dot{m} c_p \left(T_{m,o} - T_{m,i}\right)}{\left(A_s q''\right)_{tube}} * 100 \tag{2.5}$$

The two methods of heat transfer averaged a variation of 2.12%.

The numerical model was validated first by solving the unsteady laminar flow condition from a thermal plume such as a cigarette, additionally the model was used to

solve the flow and temperature field for a tube without the application of a body force (gravity) to ensure that no fluid motion was induced and subsequently the model was solved for a body force 100 times gravity to check the other extreme for any unexpected results. With the numerical model satisfactorily validated, the model was used to calculate the flow and temperature fields for vertical tubes of various length-to-diameter $\left(L/D\right)$ ratios. The calculated $\overline{Nu_D}$ was plotted against $\sqrt{Gz^{-1}}$ and compared to the correlations developed by Sieder, Tate, and Gnielinski [4,6].

D. DATA REDUCTION

Both dimensional and non-dimensional analysis methods were used to compare the results from the different models. The average heat transfer coefficient of each tube was calculated as follows:

$$Q_{conv} = \dot{m}c_p\left(T_{m,o} - T_{m,i}\right) = \bar{h}A_s\Delta T_{lm} \tag{2.6}$$

$$\bar{h} = \frac{\dot{m}c_p\left(T_{m,o} - T_{m,i}\right)}{A_s\Delta T_{lm}} \tag{2.7}$$

where

$$\Delta T_{lm} = \frac{\left(T_{m,i} - T_{m,o}\right)}{\ln\left(\frac{T_s - T_{m,o}}{T_s - T_{m,i}}\right)}. \tag{2.8}$$

The Nusselt number, $\overline{Nu_D}$, is the ratio of convective to conductive heat transfer and is defined as:

$$\overline{Nu_D} = \frac{\bar{h}D}{k_f}. \tag{2.9}$$

thus

$$\overline{Nu_D} = \frac{\dot{m}c_p\left(T_{m,o} - T_{m,i}\right)D}{A_s\Delta T_{lm}k_f}. \tag{2.10}$$

The Prandtl number, Pr, is the ratio of kinematic viscosity to thermal diffusivity and assumed to be constant. The Reynolds number, Re_D, is defined as the ratio of inertial forces to viscous forces acting on a fluid.

$$\mathrm{Re}_D = \frac{\rho u D}{\mu} \tag{2.11}$$

where

$$\dot{m} = \rho A_{cs} u. \tag{2.12}$$

Therefore the Re_D can be re-written as:

$$\mathrm{Re}_D = \frac{4\dot{m}}{\pi D \mu}. \tag{2.13}$$

The Graetz number, Gz, is used to determine the developing lengths of flow in a duct and defines as:

$$Gz = \frac{D}{L}\mathrm{Re}_D \mathrm{Pr}. \tag{2.14}$$

The local skin coefficient, $C_{f,x}$, is defined as:

$$C_{f,x} = \frac{2\tau_w}{\rho u^2}. \tag{2.15}$$

The Stanton number, St, is a modified Nusselt number defined as:

$$St = \frac{h}{\rho u c_p}. \tag{2.16}$$

The numerical models neglected radiation even though radiation has the potential to provide a significant portion of the total heat transfer when using natural convection. Therefore, the radiative heat transfer was analytically solved and included for analysis purposes where noted. Figure 4 depicts an arbitrary enclosure used to determine the effective emissivity of a partial enclosure. The radiation heat transfer was calculated as follows:

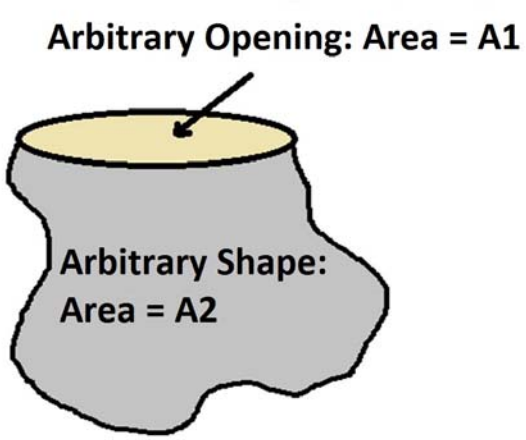

Figure 4. Arbitrary Shape and Opening Used in Radiative Analytical Analysis

$$\varepsilon_{eff} = \frac{1}{\frac{1}{\varepsilon_2} - \left(\frac{1}{\varepsilon_2} - 1\right)\left(1 - \frac{A_1}{A_2}\right)} \tag{2.17}$$

$$Q_{rad} = \sigma \varepsilon_{eff} A_1 \left(T_s^4 - T_\infty^4\right). \tag{2.18}$$

Therefore, the total heat transferred was the summation of Q_{conv} and Q_{rad}:

$$Q_{tot} = Q_{conv} + Q_{rad}. \tag{2.19}$$

The thermal resistance, R_{Th}, for the evaluated heat sinks was determined as:

$$R_{Th} = \frac{T_s - T_\infty}{Q_{tot}}. \tag{2.20}$$

The thermal entrance length is the distance from the entrance where the heat flow is fully developed (e.g., for constant temperature heating) $\overline{Nu} = 3.66$ and is calculated using the equations discussed by Rathore and Kapuno [15], where the Re_D is obtained from eqn. 2.13.

$$\text{Laminar Flow: } \frac{L_e}{D} \approx 0.05\,\mathrm{Re}_D\,\mathrm{Pr} \tag{2.21}$$

$$\text{Turbulent Flow: } \frac{L_e}{D} \approx 10 \tag{2.22}$$

The thermal entrance length was then used to calculate the percentage of the thermal entrance length the tube utilized for flow development before being broken up by the next gap. The percentage of the thermal entrance length was calculated as follows:

$$\% \text{ of Thermal Entrance Length} = \frac{L}{L_e} * 100 . \qquad (2.23)$$

The velocity entrance length was not calculated since the working fluid is air (Pr = 0.707) the thermal boundary layer will develop much faster. The thermal entrance length will be approximately 60% that of the velocity entrance length.

III. RESULTS AND DISCUSSION

A. SINGLE TUBE AND MULTIPLE STACKED TUBES COMPUTATIONAL RESULTS

The numerical computations were performed for a range of governing parameters shown in Table 1. The length-to-diameter(L/D), gap-to-length (G/L) and number of tubes were varied and all additional variations are a direct result of the manipulation of these three parameters.

Table 1. Governing Parameters

L/D	0.133–300
G/L	0.033–2
$\overline{Nu_D}$	6.1–24.3
Re_D	358–3151
Gz	7.4–4502.9
Pr	0.707
$T_s - T_\infty$	73 ^oK

1. Effect of Length-to-Diameter Ratio, L/D

For a single vertical tube, the length of the tube plays a vital role in the fluid flow and heat transfer characteristics of the tube. As the L/D ratio increased, the mass flow rate through the tube increases, which in turn increases the Re_D. As the Re_D increases, the thermal entrance length for the tube increases; however, as shown in Figure 5, the length of the tube increases faster than the thermal entrance length therefore a larger percentage of the entrance length was used by the flow, which resulted in a smaller $\overline{Nu_D}$ for the tube.

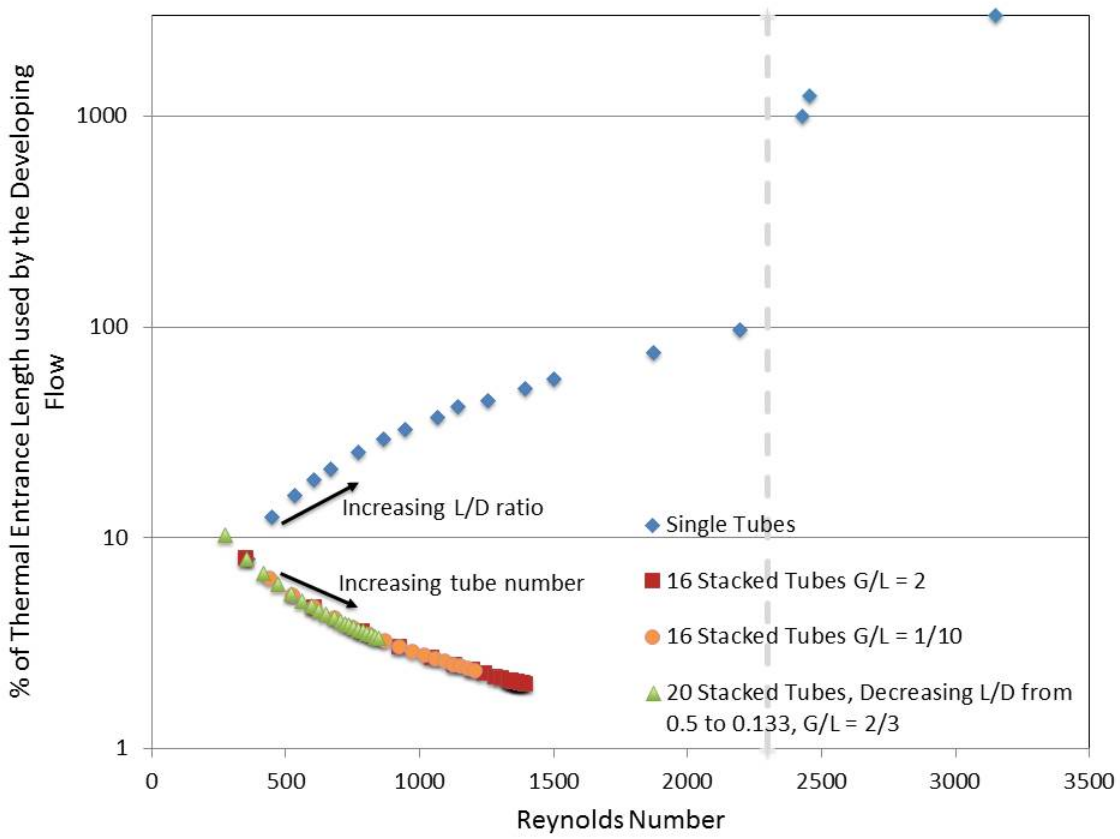

Figure 5. Percentage of Thermal Entrance Length used by the Developing Flow vs. Reynolds Number

When plotting the determined $\overline{Nu_D}$ versus $\sqrt{Gz^{-1}}$ the single tube models trend with the Sieder and Tate correlation for laminar flow in a combined entrance length until the flow transitions to turbulent [4]. Only one geometry depicted flow that is fully turbulent and developed, but in that one case the $\overline{Nu_D}$ versus $\sqrt{Gz^{-1}}$ agrees with the Gnielinski correlation [6]. These results are plotted in Figure 6.

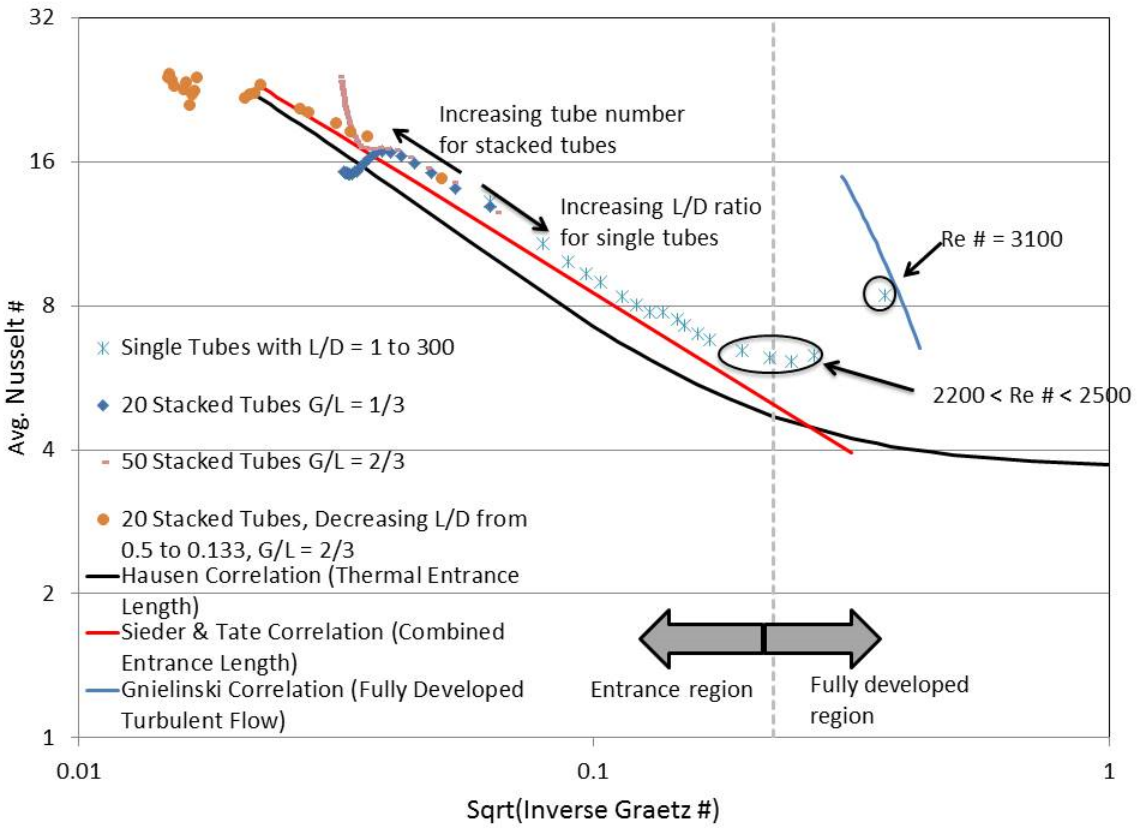

Adapted from correlations developed by Sieder and Tate, Gnielinski, and Hausen [4–6].

Figure 6. Average Nusselt Number vs. Square Root Inverse Graetz Number

2. Effect of Stacked Tubes

Based on the results from single vertical tubes an $L/D = 1$ was selected for the majority of the investigations into stacking multiple tubes. When the tubes are aligned vertically the moving fluid exiting a tube is at a slightly lower pressure than the ambient air surrounding the gap causing it to be drawn in and entrained in the moving fluid. This forces the moving fluid from the previous tube to utilize a smaller cross-sectional area as the entrained ambient air develops the new boundary layer thus resulting in an increase of the mass flow rate through each additional tube. The left graphic in Figure 7 depicts the fluid streamlines compressed by the ambient air entrained in the vertical tube system. The right graphic depicts the same streamline with the addition of the wall heat flux.

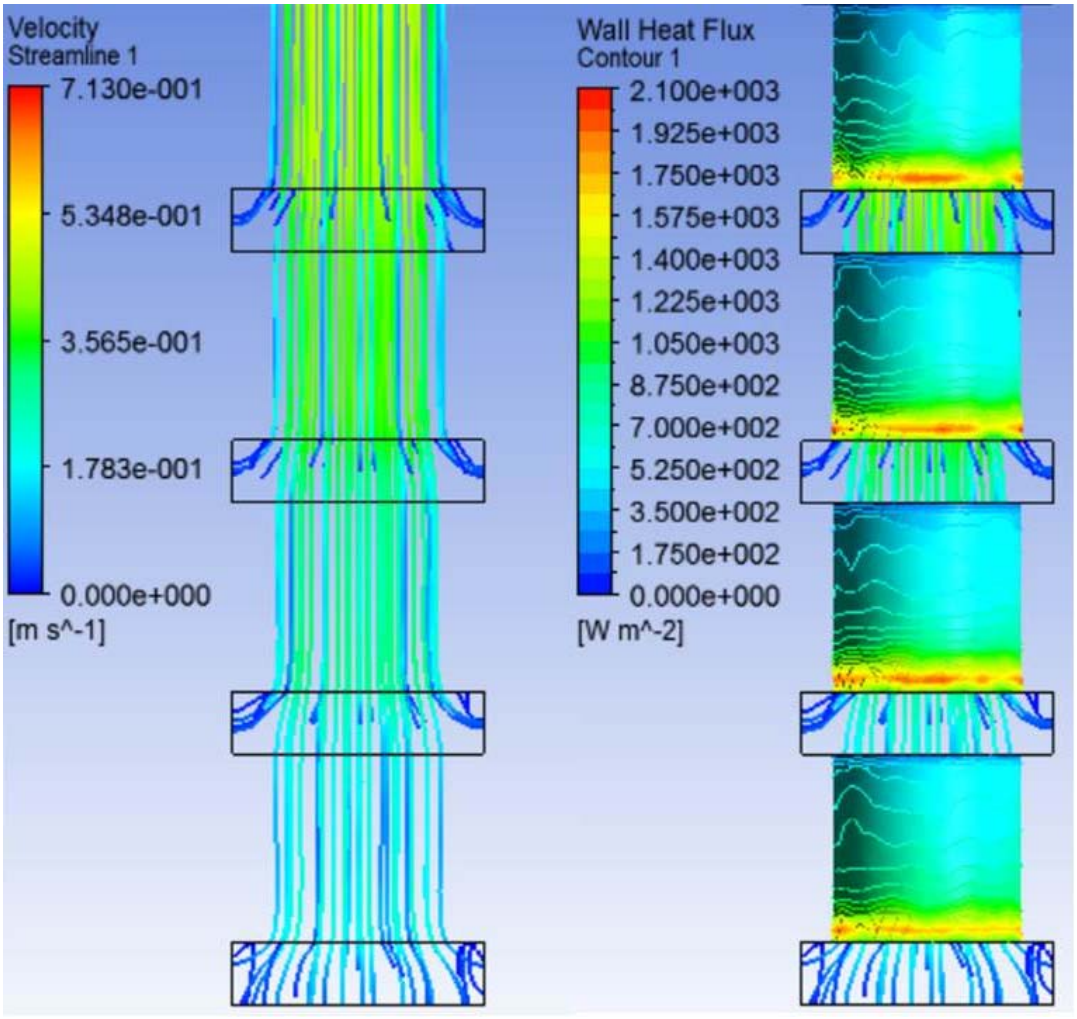

Figure 7. Streamlines of Stacked Tube Model with Wall Heat Flux

Interesting trends in the heat transfer characteristics are revealed when the $\overline{Nu_D}$ is calculated for each tube. The $\overline{Nu_D}$ increases through each tube as depicted in Figure 6 plotted alongside the single tube results, the Sieder and Tate correlation (combined entry region), the Hausen correlation (thermal entry region), and the Gnielinski correlation (fully developed turbulent flow) [4–6]. There are multiple contributing factors that result in an increase of the $\overline{Nu_D}$.

- The thermal and velocity boundary layers are disrupted due to the gap between tubes therefore the boundary layers have to re-develop. This is shown by the calculated $\overline{Nu_D}$ for each tube trending with the Sieder and Tate [4] correlation for a combined entry region. This can also be seen in Figure 7 by the streamlines of the ambient fluid and the tube wall heat flux contours.

- The entrainment of the surrounding air near the gap increases the mass flow rate, which in turn increases the length of the thermal development region. Since the tube length is maintained constant the percentage of the entrance length utilized decreases, as seen in Figure 5, resulting in an increase of the $\overline{Nu_D}$.

- The local skin friction coefficient, $C_{f,x}$, is a maximum at the entrance of a round tube and decreases to a horizontal asymptote. The skin coefficient can be used to relate the wall shear stress to heat transfer through the Reynolds Analogy, $\frac{C_f}{2} = St$, which can be used to solve for the heat transfer coefficient to rewrite the heat flux as $q_s^{"} = \frac{\tau_s c_p (T_s - T_\infty)}{u}$. This results in both the shear stress and the heat transfer being a maximum at the entrance of each tube, as depicted in Figure 8.

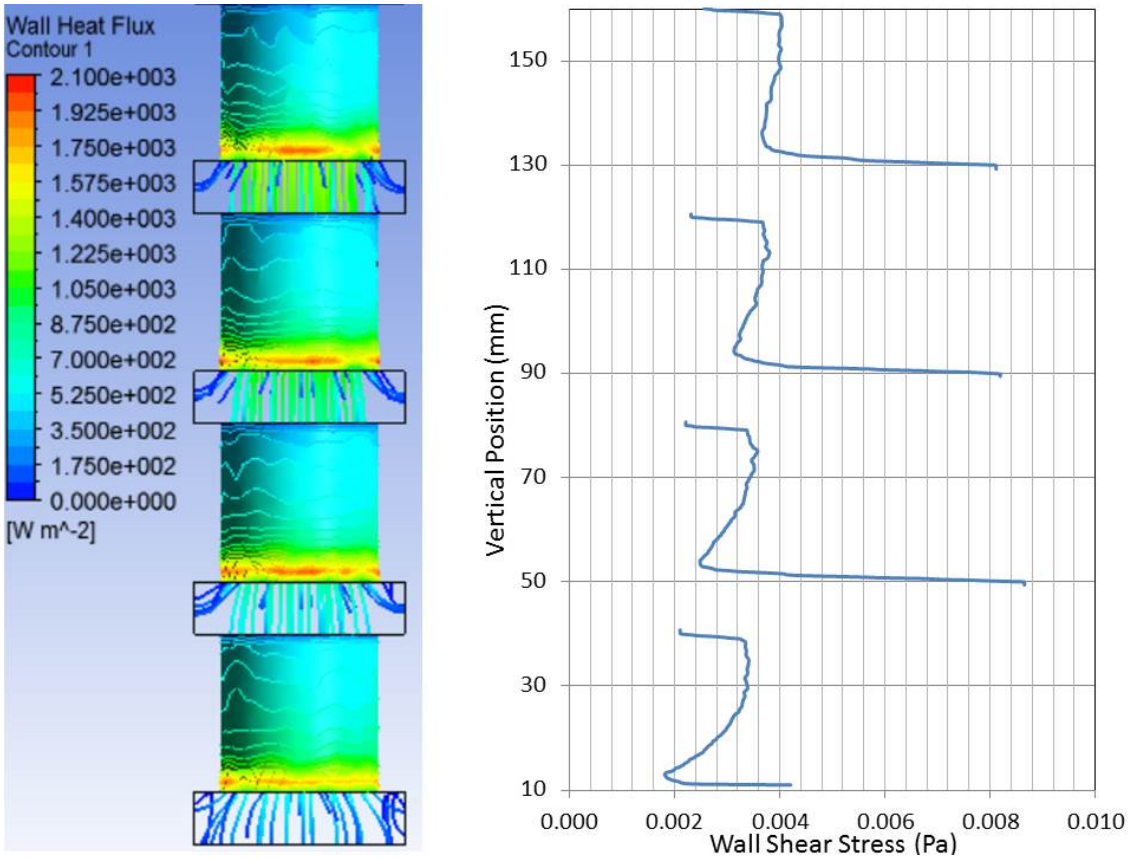

Figure 8. Stacked Tube Model with Associated Wall Shear Stress Plot

3. Effect of Gap-to-Length Ratio, G/L

A series of geometries consisting of 4, 8, 12, 16, and 20-stacked tubes with the G/L ratio varied from 1/30 to 2 was analyzed. One additional model consisting of 50-stacked tubes was analyzed to assess for a potential maximum. The G/L ratio has a significant impact on the heat transfer characteristics of the system. When the G/L ratio is too small, the stacked tubes act similar to a single tube, where the $\overline{Nu_D}$ through each subsequent tube decreases. That trend was only observed when the G/L = 1/30. As the G/L ratio is increased closer to 2, there is almost no degradation in the amount of heat transferred from one to the next.

The multiple stacked tubes with a constant L/D = 1 diverged from the Sieder and Tate [4] correlation. The break from the previously established trend was assessed to

be dependent on the Re_D. Figure 9 plots $\overline{Nu_D}$ versus Re_D and shows an inflection point at Re_D equal to 1150.

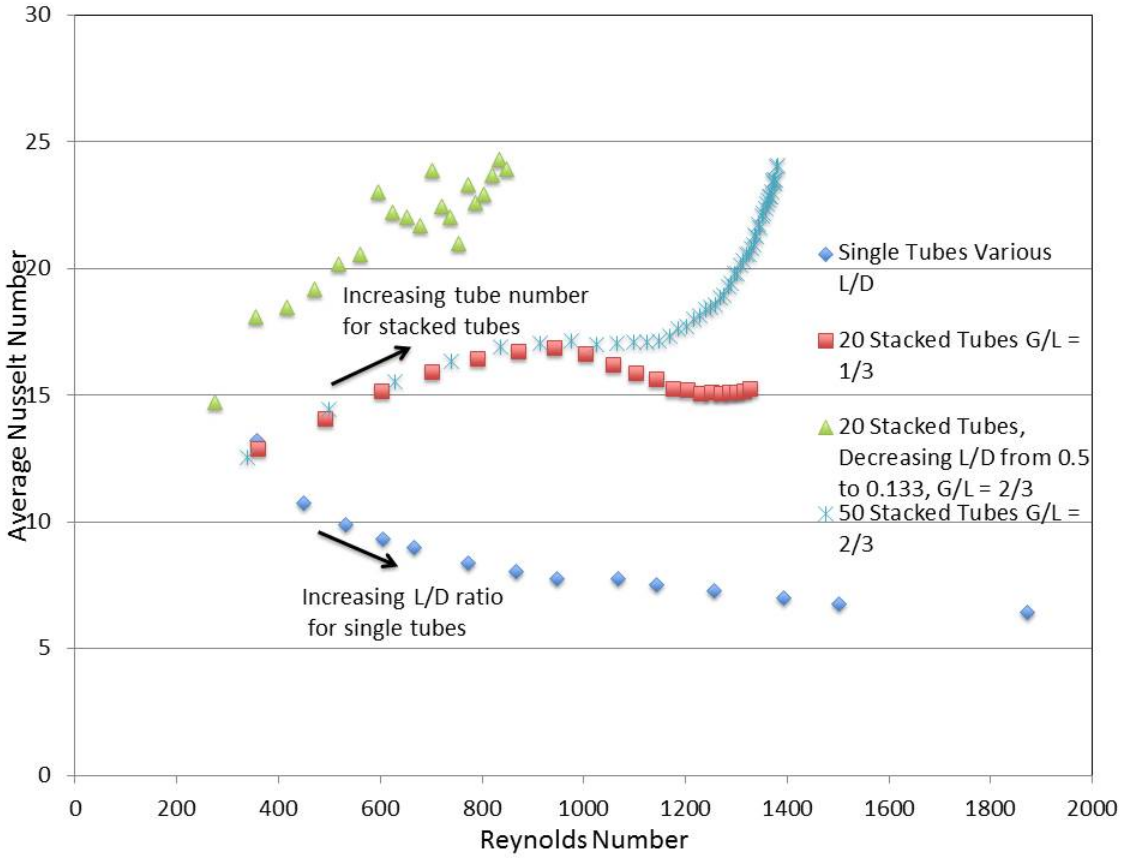

Figure 9. Average Nusselt Number vs. Reynolds Number

The nature of the shift is dependent on the G/L ratio. When the G/L = 1/3 the trend appears to shift down and follow the Hausen [5] correlation for the thermal entrance length of a pre-developed velocity profile. Figure 10 shows the velocity profile for the first, second, ninetieth and twentieth tubes. It is observed that the entrance velocity profile is undeveloped in the earlier tubes but in the later tubes, the entrance velocity profile shows the characteristics of a developed flow.

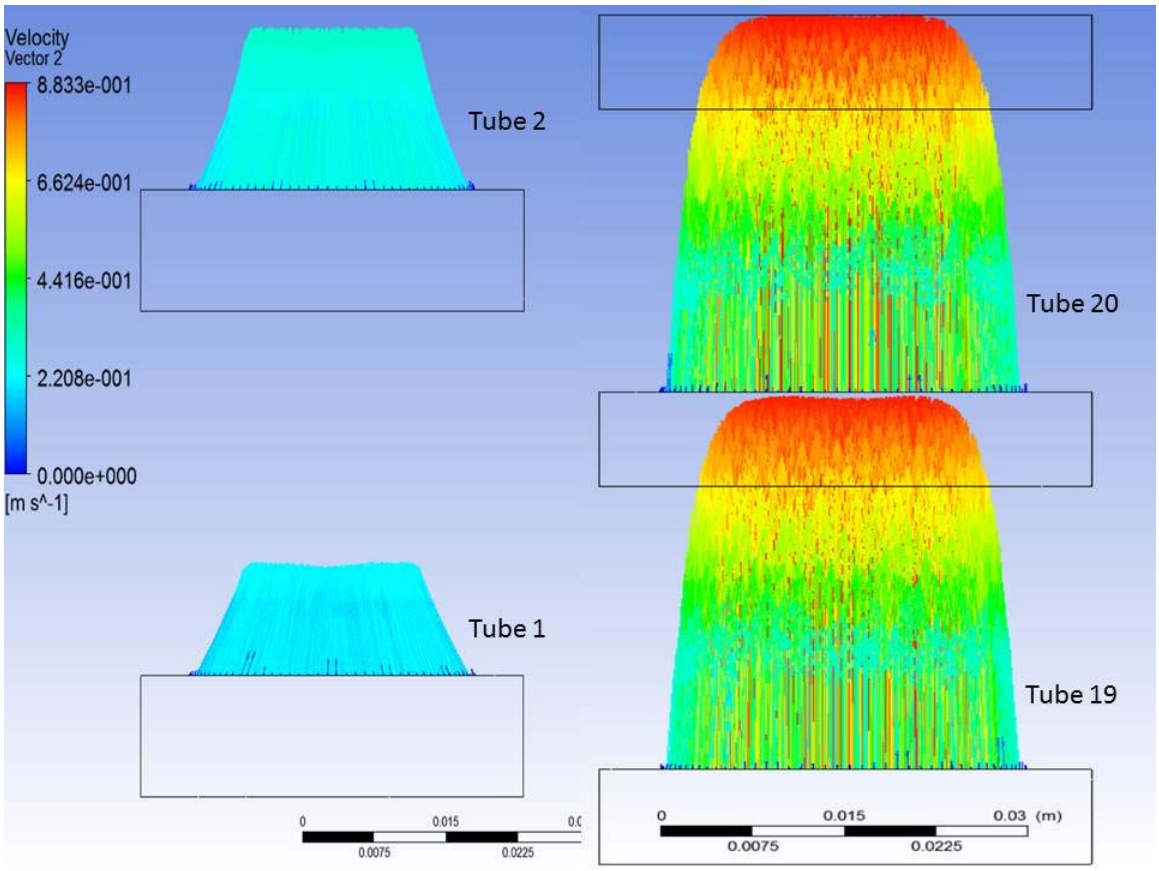

Figure 10. Velocity Profiles for 20-Stacked Tubes

However, for a G/L = 2/3 the divergence breaks in a different direction. Figure 11 shows the entrance and exit velocity profile for the fiftieth tube, which shows an atypical entrance velocity profile. The entrance velocity profile has a star pattern to the velocity distribution but by the exit of the tube, the velocity profile displays a more typical developed velocity profile. This star pattern appears to be a result of both the G/L ratio and the tube entrance geometry.

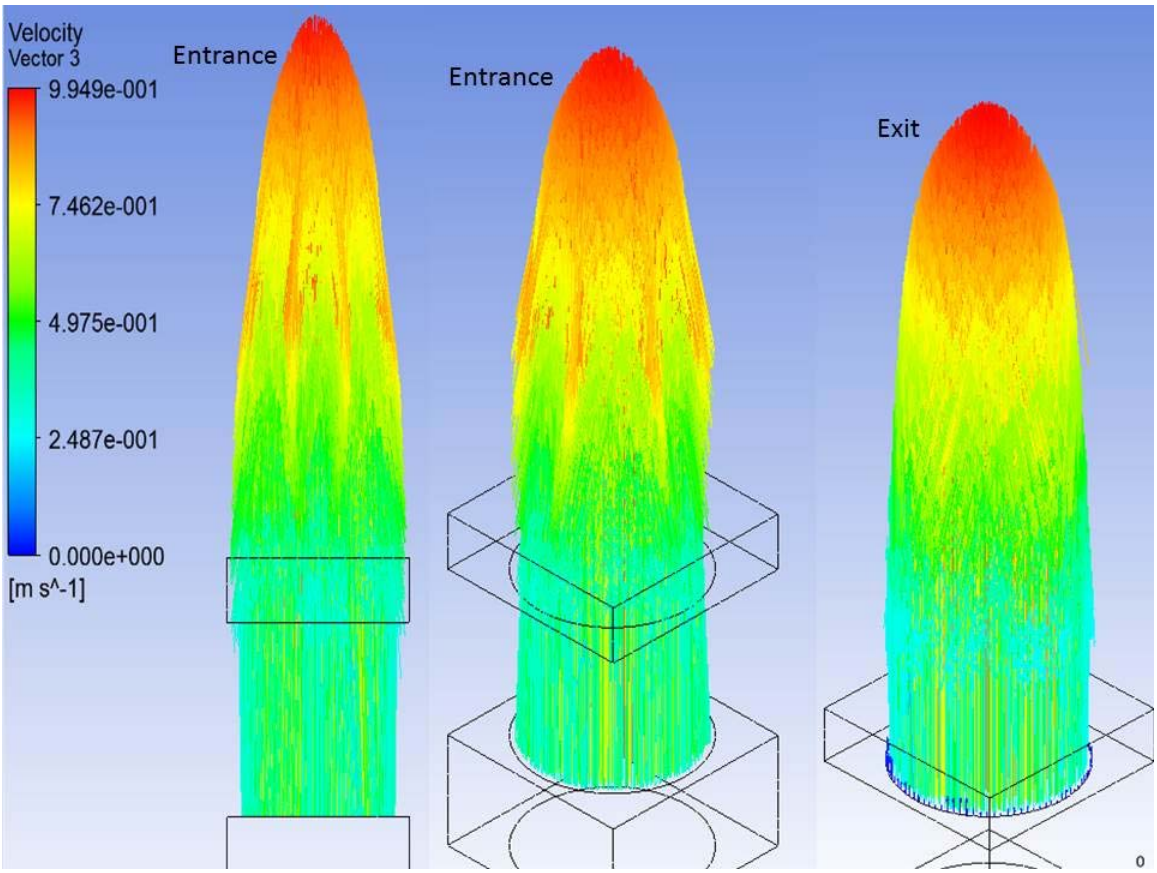

Figure 11. Velocity Profiles for the 50-Stacked Tubes

The additional G/L ratios evaluated diverge at the same Re_D; however, they fan out depending on the G/L ratio. Figure 12 depicts the divergence for multiple G/L ratios but these results were obtained from models with a mesh not as refined as depicted in Figures 6 and 9. Sample mesh sizes are tabulated in Appendix A.

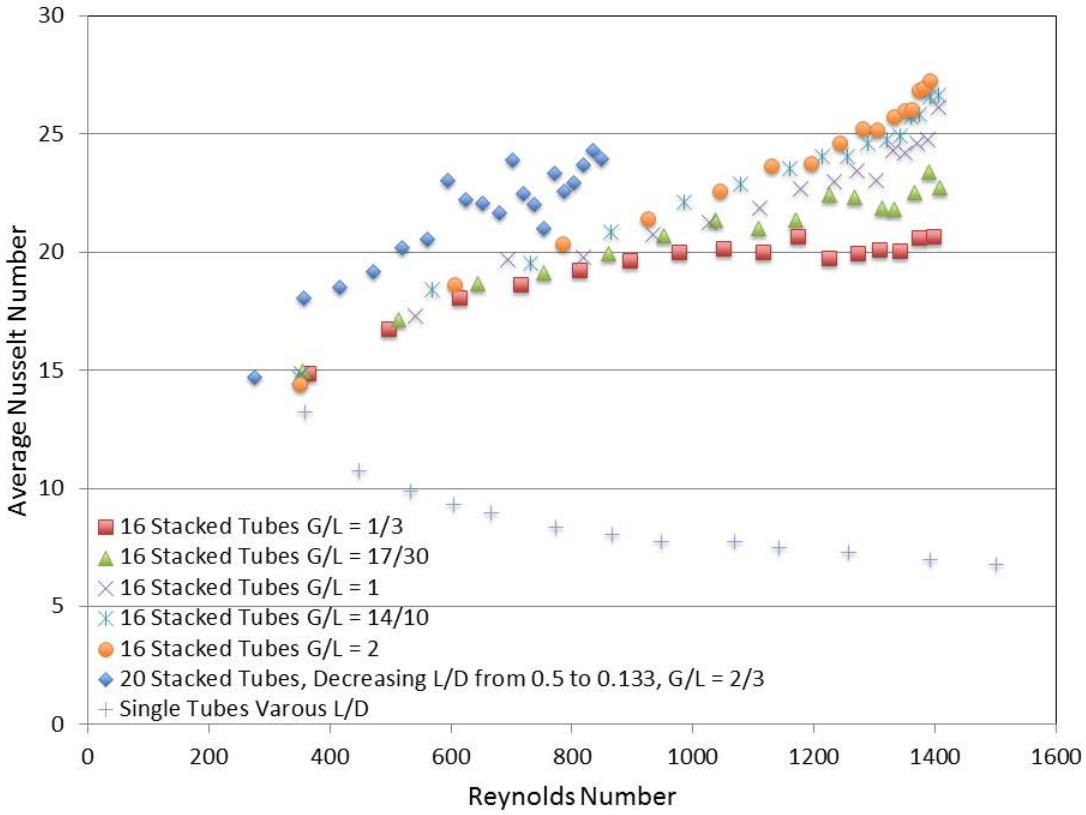

Figure 12. Average Nusselt Number vs. Reynolds Number for Less Refined Mesh

The optimal G/L ratio was determined by dividing the total heat transferred from the system by the summation of the length of the individual tubes and gaps and plotted against the G/L ratio for the different stacked tube systems. If the goal is to maximize heat transfer in a small overall length the use of smaller gaps will be optimal; however, for larger overall lengths the use of larger gaps are optimal since the larger gap reduces the degradation of heat transfer from one tube to the next. Therefore, the optimal G/L ratio is dependent on the overall length of the tube system. Figure 13 depicts this trend by plotting the normalized heat transfer per unit length for the various G/L ratios.

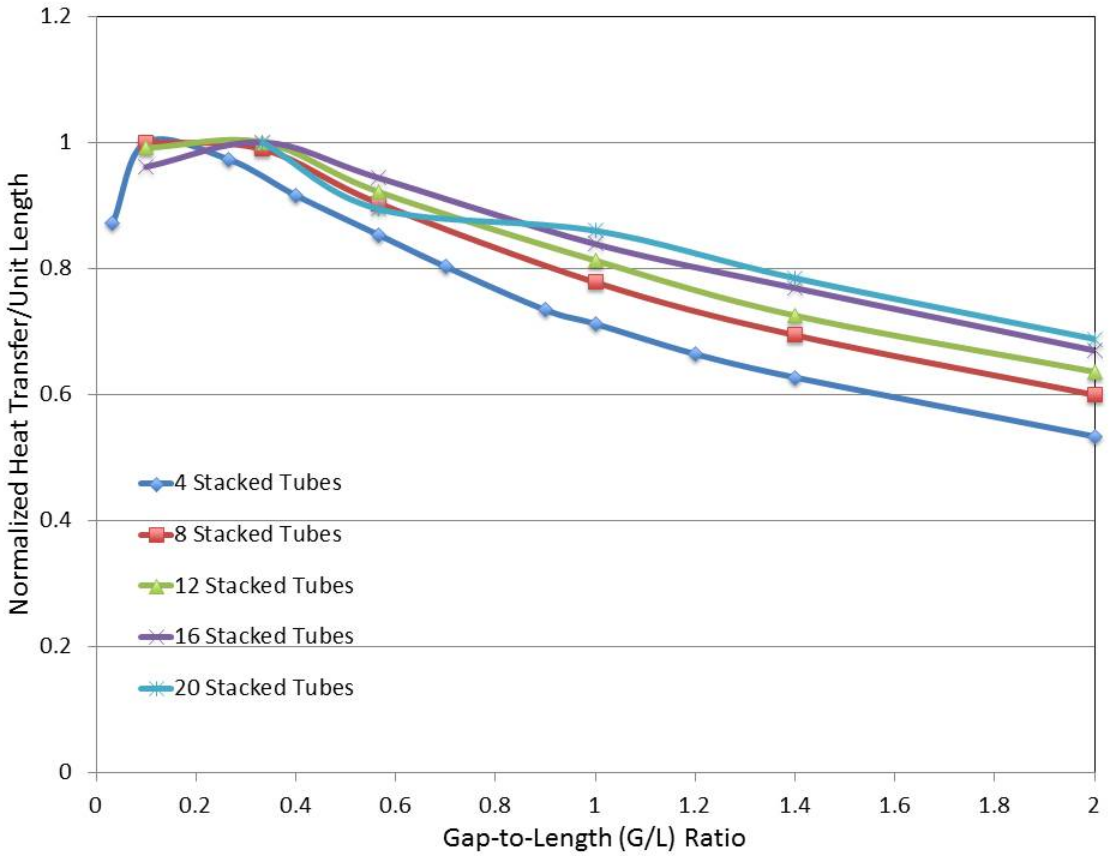

Figure 13. Normalized Heat Transfer per Unit Length vs. Gap-to-Length Ratio

The results of the heat transferred from the stacked tubes was plotted to compare to the heat transferred from a single tube with the same total length. From Figure 14, it becomes apparent that if the G/L ratio is too large the heat transfer will be worse than that of a single tube with the same total length. This was only observed in the 4-stacked tube systems, since the G/L ratio where the overall performance becomes worse increases as the number of tubes in the stacked tube system increases. It is also observed that a stacked tube system can be used to transfer the same amount of heat energy with the use of a portion of the length that would be required of a single tube, in some cases the stacked tubes would only need ~55% the total length of a single tube to transfer the same amount of heat. In Figure 14, the heat transfer was plotted against the total length of the system. For instance, the 8-stacked tubes with the smallest G/L ratio will result in the

smallest total length; therefore, will be the farthest left data point. This is the same for all multiple stacked tube systems plotted.

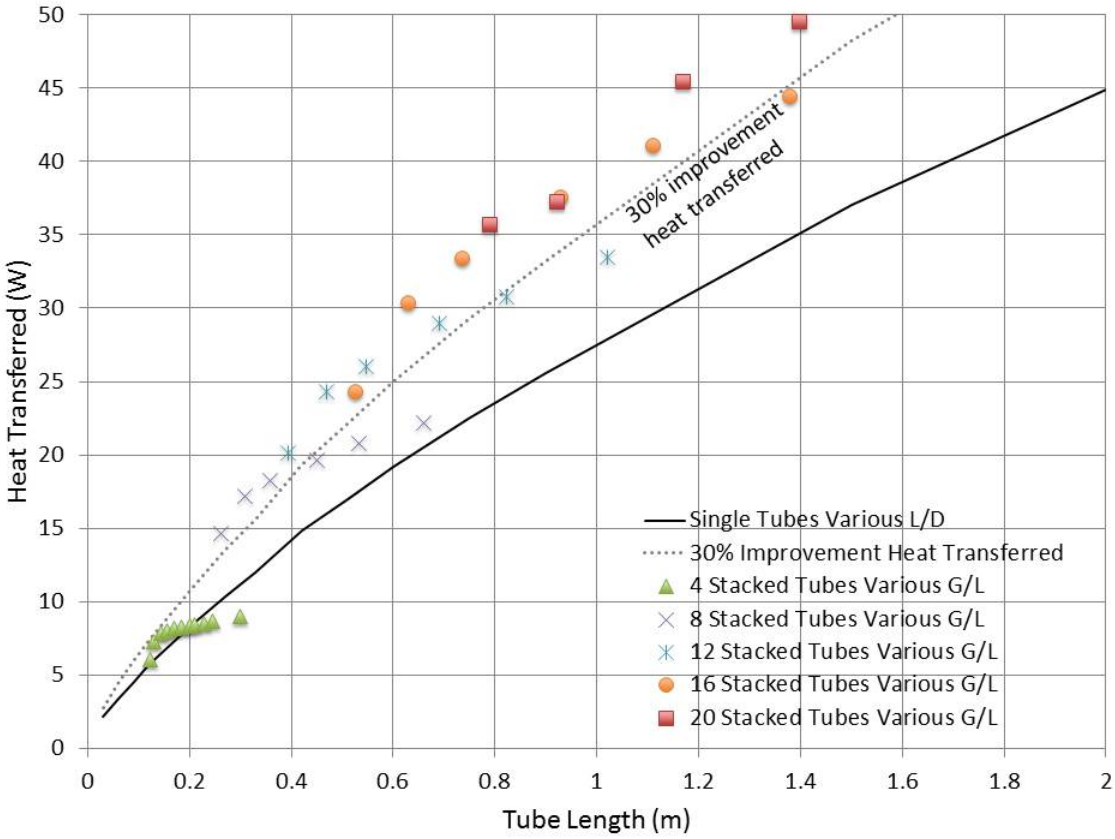

Figure 14. Heat Transfer versus Total Length of the System

B. TUBE SYSTEM VERSUS PIN-FIN HEAT SINK COMPUTATIONAL RESULTS

Based on the insight gained from analyzing stacked tube systems, three heat sinks were created with a base of 15cm x 15cm with a height of 20cm. Circular pin-fin heat sinks were created with the same spacing and outer diameter for comparison. Two additional 64 pin-fin heat sinks were created to have a surface area range that encompassed the range of the tube system heat sinks. Table 2 shows the surface area for each heat sink evaluated and in the subsequent figures the data will be plotted against the surface area.

Table 2. Surface Area for Each Evaluated Heat Sink

# Fins	1	5	9	16	25	64	64 (mod)
Pin-Fin Surface Area (m^2)	0.096	0.154	0.193	0.299	0.344	0.382	0.502
Tube System Surface Area (m^2)	0.187	0.303	0.396	0.476	0.565	N/A	N/A

1. Effects of Pin-Fin versus Tube System

The convective and radiative heat transfer was plotted for each heat sink geometry versus the surface area in Figure 15. Based on the polynomial curve fit the 9- and 16-tube systems show an 18% and 19% improvement in the convective heat transfer over an equivalent surface area pin-fin heat sink. The 9-tube system heat sink shows a 118% improvement over the 9-pin-fin heat sink. As the number of tube systems increases the heat transfer improvement diminishes when compared to an equivalent surface area pin-fin heat sink. This indicates that the tube system geometry has an optimal point and loses its effectiveness as the number of tube systems continues to increase. This offers an explanation to why Awad, whose experiments consisted of 95 staggered or 100 in-line hollow pin-fins, concluded that hollow pin-fins perform more poorly than solid pin-fins, while Elshafei used 8 hollow pin-fins and determined that hollow pin-fins outperform solid pin-fins [10,11].

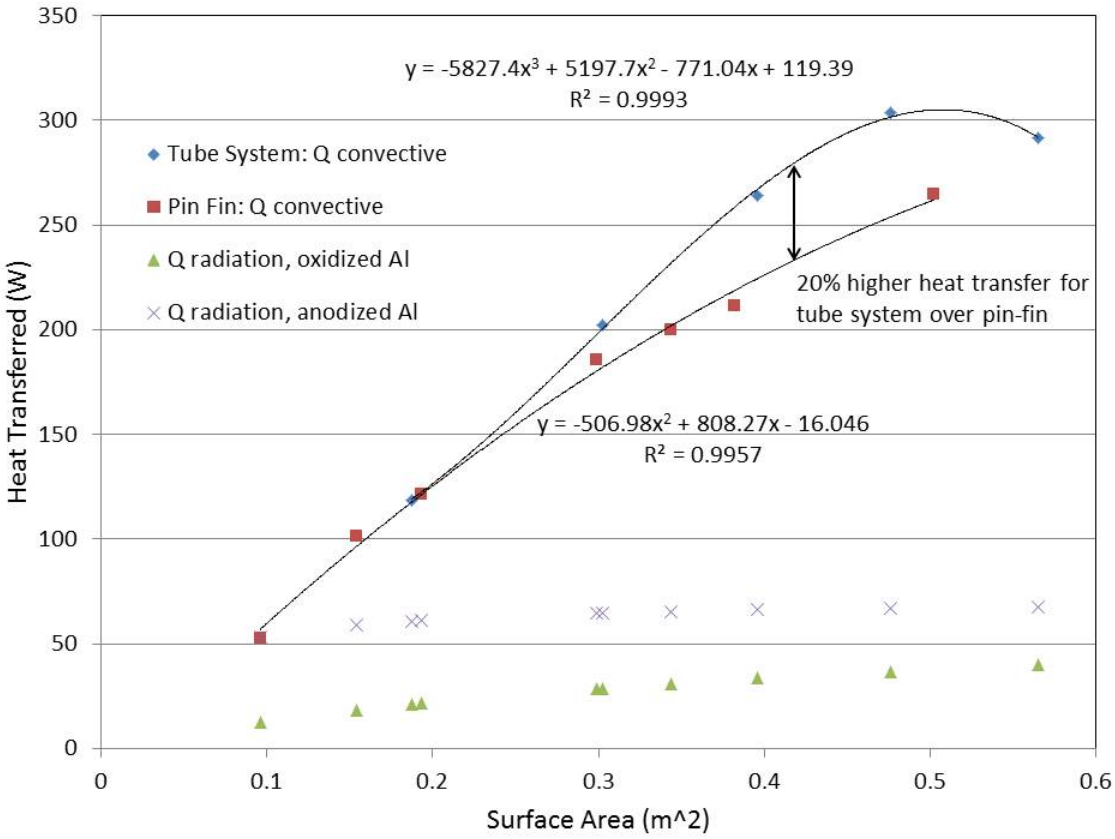

Figure 15. Heat Transferred vs. Surface Area

Figure 16 depicts the average convective heat transfer coefficient for each heat sink and clearly shows that the upward oriented tube system has a higher average heat transfer coefficient when compared to pin-fins. This verifies that the geometric structure of a stacked tube system enhances the overall heat transfer characteristics of the heat sink and not only due to the additional surface area. The increased heat transfer coefficient is caused by two effects: 1) the disruption of the thermal and velocity boundary layers due to the gaps in the tubes and 2) the creation of a stack effect by vertically aligning the tubes that causes cooler ambient air to be drawn into the heat sink

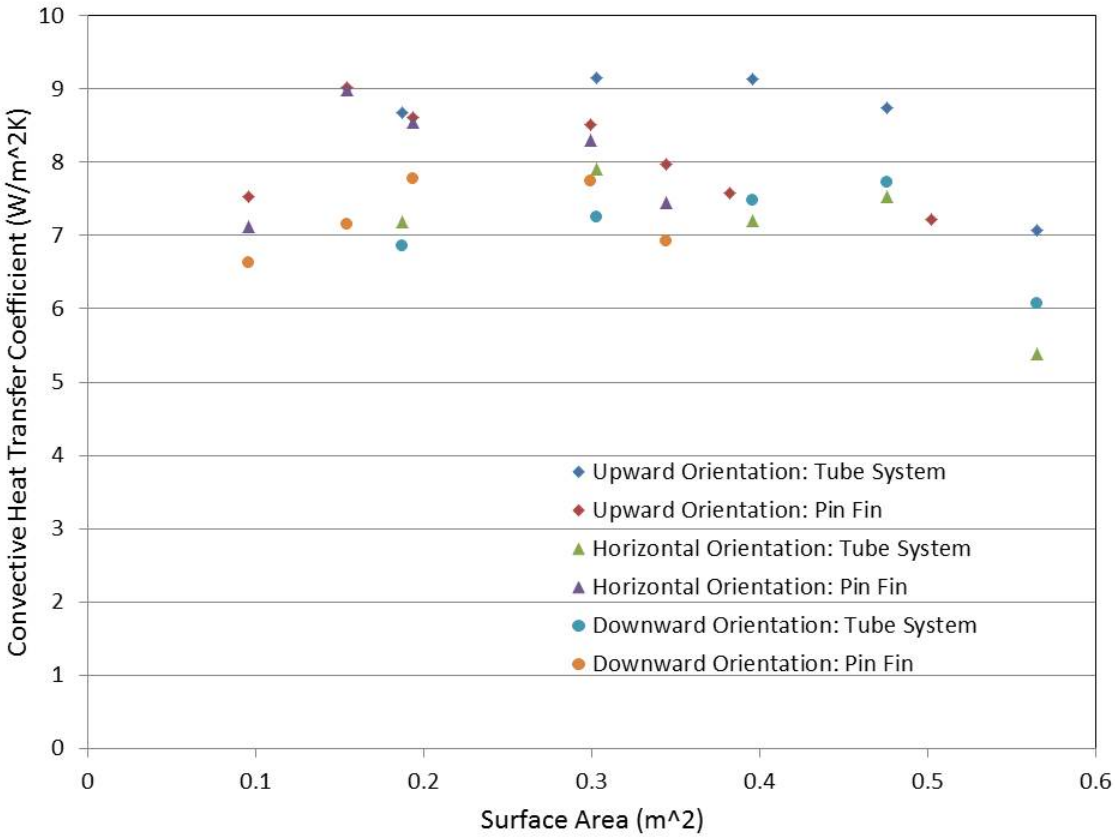

Figure 16. Convective Heat Transfer Coefficient vs. Surface Area

2. Effects of Orientation

The various heat sinks were analyzed in three orientations: the fins pointing upward, the fins pointing downward, and the fins pointing horizontal. Figure 17 depicts the convective heat transfer versus surface area for each of the orientations. Based on the changes of the heat transferred due to orientation it becomes apparent that the tube systems are more greatly affected by orientation than the pin-fin heat sinks.

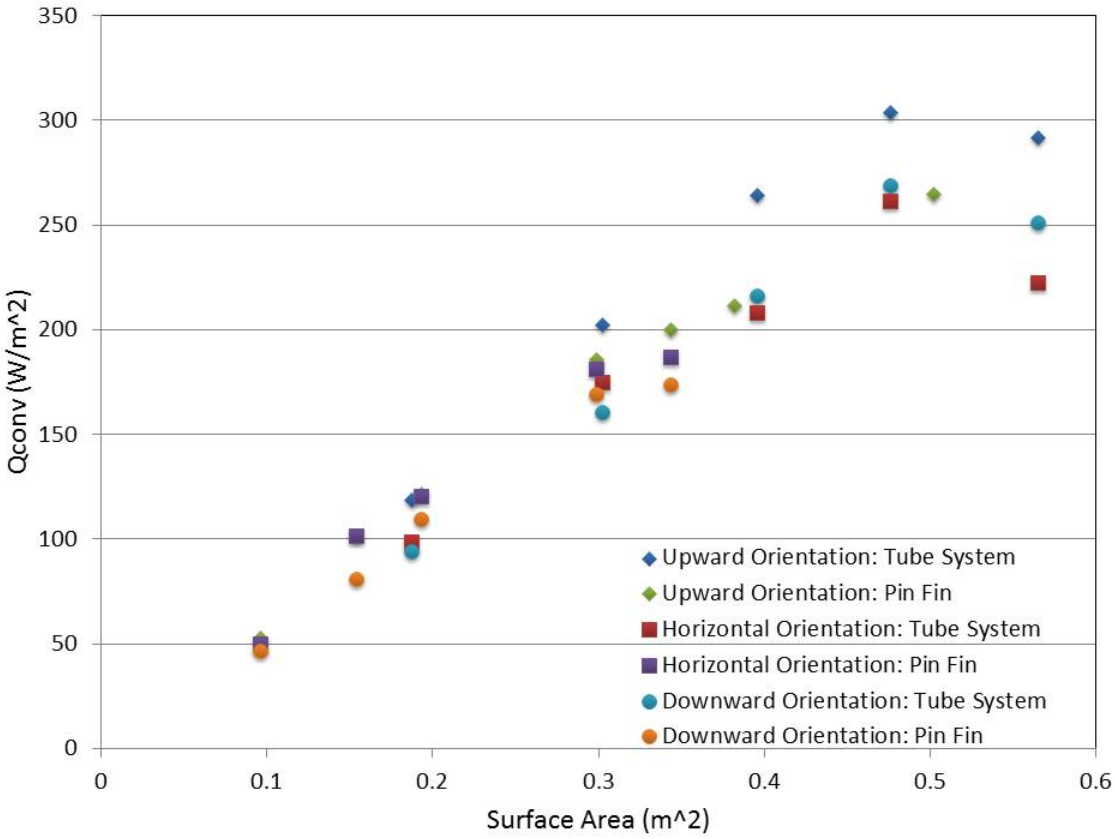

Figure 17. Convective Heat Transfer vs. Surface Area

The results of the pin-fin heat sinks correlates with results previously published by Sertkaya et al., Huang et al., and Elshafei that horizontal pin-fins can be comparable to upward oriented pin-fins, depending on the pin-fin arrangement, while the downward facing pin-fin heat sink yields the lowest heat transfer capability [8–10]. Contrary to the pin-fin heat sinks, the downward facing tube systems provide a better heat transfer capability than the horizontal tube systems. Figure 18 depicts the normalized heat transfer based on orientation.

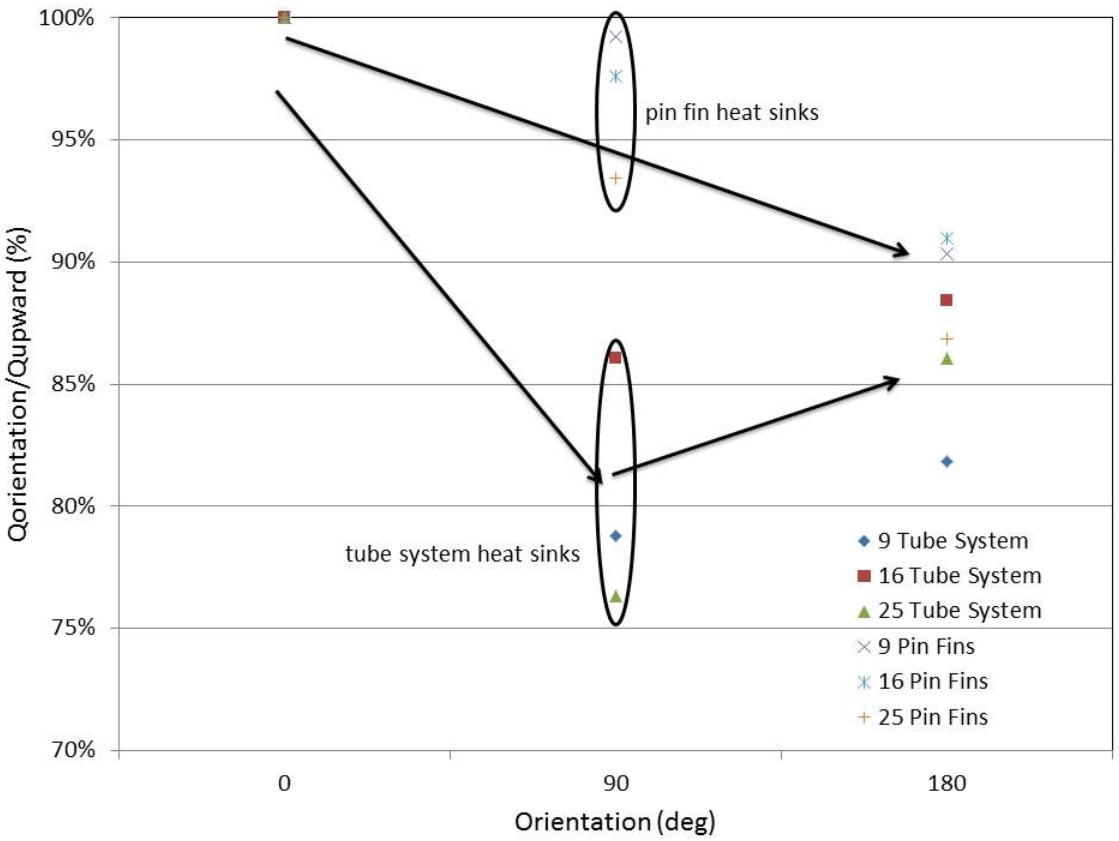

Figure 18. Normalized Heat Transfer Based on Orientation

Figure 19 plots the thermal resistance of the different heat sinks evaluated at different orientations versus the surface area. This shows that the tube system heat sinks have a lower thermal resistance than the pin-fin heat sinks and the 16-tube system has the lowest thermal resistance.

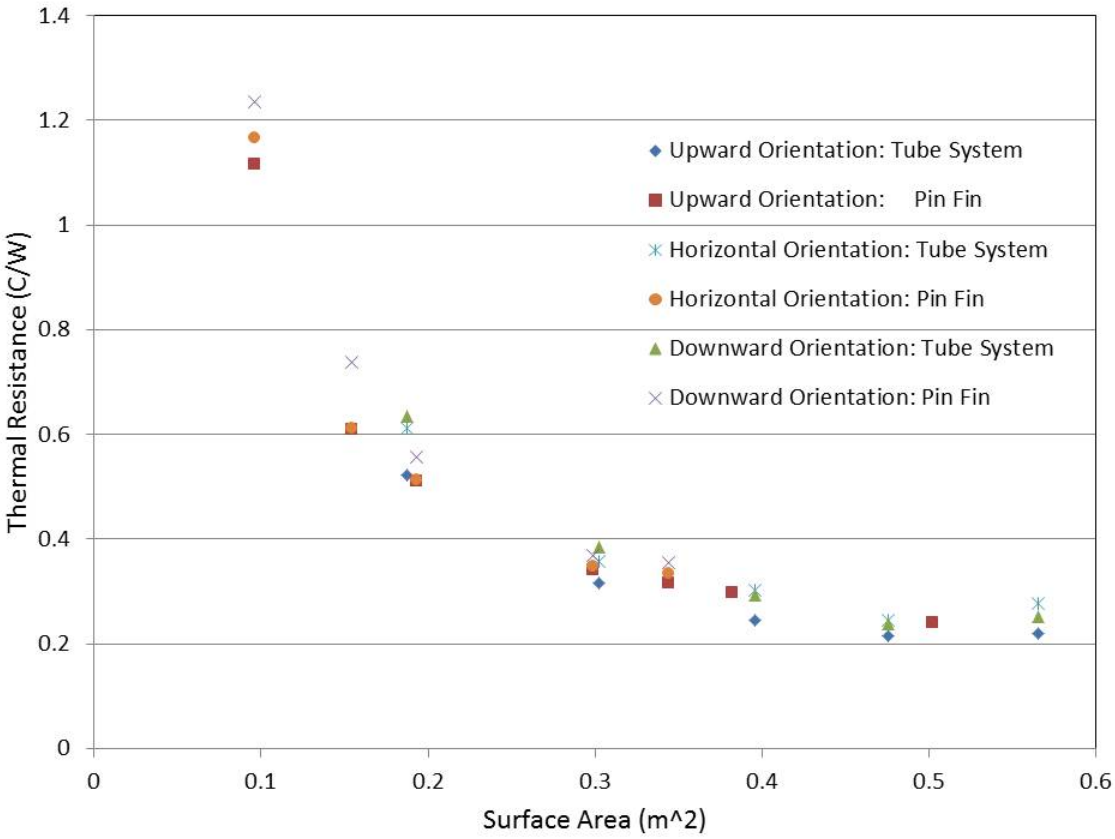

Figure 19. Thermal Resistance vs. Surface Area for the Various Orientations

3. Effects of Additional Appendages

Based on the streamlines in the 16-tube system heat sink, as shown in the upper left and right of Figure 20, additional features were evaluated for any additional heat transfer enhancements. The placement of the additional appendages is shown in the lower picture of Figure 20. The purpose of this was to evaluate if impingement cooling could be utilized by placing an extrusion perpendicular to the streamline in certain locations. Two additions were evaluated both separately and combined: impingement fins and a center X.

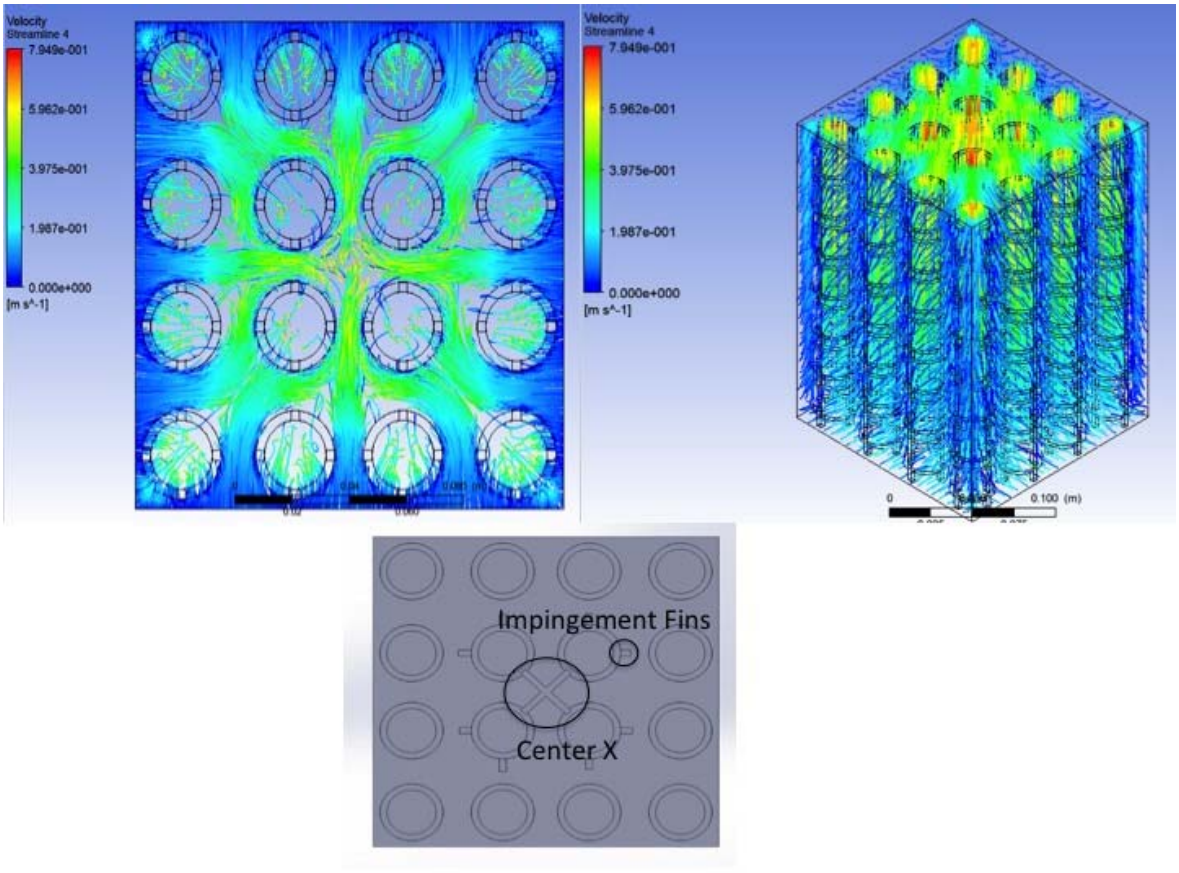

Figure 20. Fluid Streamlines and Location of Additional Appendages

The result from the different combinations of the additions reveals a reduction in the heat transfer capability of the heat sink with the exception of the downward facing tube system. The results are graphically depicted in Figure 21.

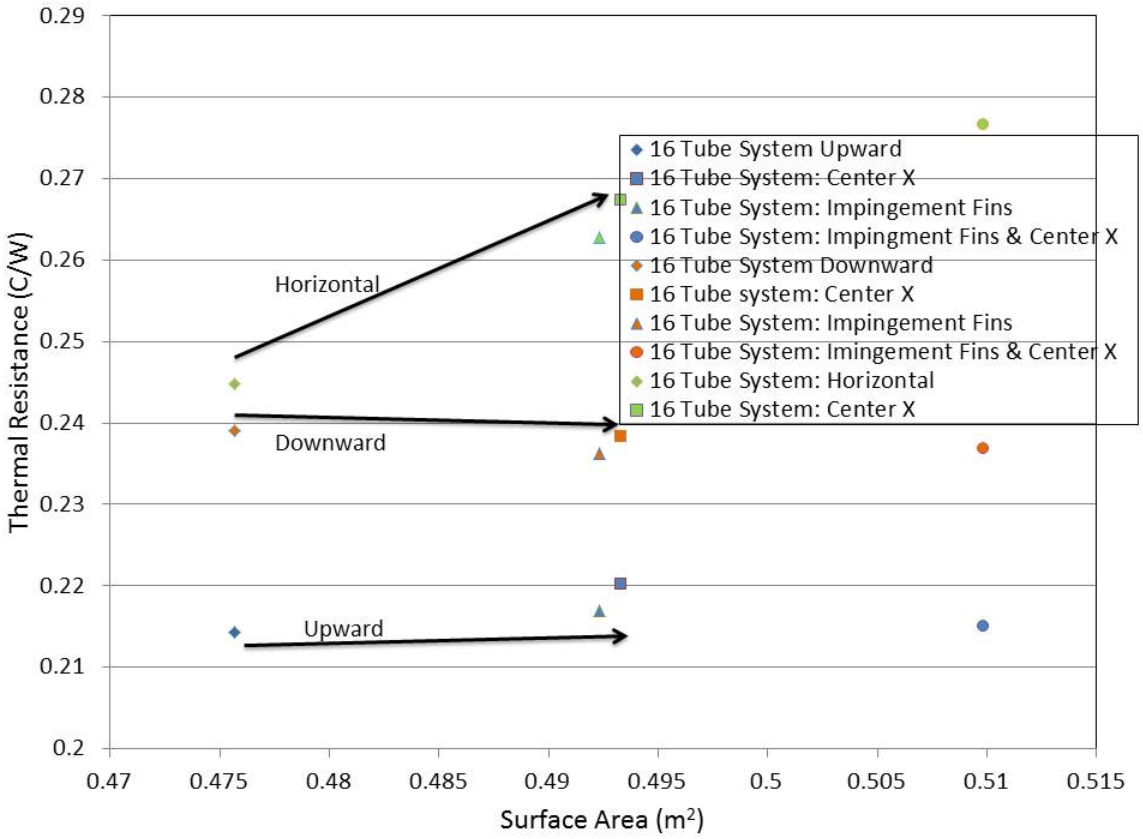

Figure 21. Comparison of Thermal Resistances for the Different Additional Appendage Combinations

IV. CONCLUSIONS

Heat transfer and fluid flow characteristics from vertically aligned tubes were examined numerically. The effects of the length-to-diameter ratio, number of stacked tubes, and gap-to-length ratio on the heat transfer and fluid flow were studied.

The numerical results closely follow the previously established correlations of Sieder and Tate for the combined entry length under laminar flow conditions. It was observed that the gap between the tubes breaks up the thermal and velocity boundary layers. The cooler ambient air near the gap becomes entrained in the fluid exiting the tube causing the mass flow rate and average Nusselt number to increase through each subsequent tube. The effects on the heat transfer and fluid flow characteristics are dependent on the number of stacked tubes, gap-to-length ratio, and the length-to-diameter ratio. It was numerically demonstrated that a stacked tube system with a total length 55% of a single tube could transfer the same amount of heat.

The insight gained was utilized to develop novel heat sinks to compare to circular pin-fin heat sinks. The effect of number of fins and orientation on the heat sinks was additionally analyzed. The tube system heat sink outperforms the pin-fin heat sink; however, that is dependent on the number of tube systems utilized. If the number of tube systems is too great, the performance will actually be worse than an equivalent surface area pin-fin heat sink. The 16-tube system heat sink provided the lowest thermal resistance and highest average heat transfer coefficient out of all of the heat sinks analyzed. The orientation of a tube system heat sink is more drastically affected by the orientation than pin-fins but contrary to the pin-fin heat sinks the downward facing tube system outperforms the horizontal tube system with the upward facing tube system offering the best heat transfer capability. An upward facing tube system heat sink has been shown to provide a 20% increase in the heat transfer capability over an equivalent area pin-fin heat sink.

The results of this numerical study show that there are geometric structures that can be incorporated to improve the overall heat transfer capability of a system subjected

to natural convection. In this specific study, a tube system heat sink was shown to outperform a circular pin-fin heat sink. There is still further progress that can be made by optimizing the spacing between tube systems, the alignment of the systems (e.g., in-line versus staggered), and the entrance and exit geometry of each tube in the tube system. An experimental validation of these results was conducted with the results discussed in Appendix B.

Upon the conclusion of this study, Plunkett Associates used a Direct Metal Laser Sintering process to construct novel heat sinks that could not be created using traditional manufacturing processes [16]. These novel heat sinks demonstrated a significant improvement in heat transfer over typical extruded heat sinks. The importance of this press release validates the assumption that unused geometric structures exist that can be utilized to increase the natural convection capability of heat sinks and companies are starting to explore the possibilities.

APPENDIX A. ANSYS MESH AND PHYSICS REPORTS FOR VARIOUS GEOMETRIES.

A. ANSYS PHYSICS REPORT

Table 3. 20-Stacked Tubes ANSYS Physics Report

Domain	**Boundaries**	
chimney20tubes	**Boundary – open_boundary**	
	Type	PRESSURE-OUTLET
	Boundary – tube (heat source)	
	Type	WALL
	Boundary – wall chimney20tubes (adiabatic walls)	
	Type	WALL

B. ANSYS MESH REPORT

Table 4. Various ANSYS Mesh Reports

Domain	Nodes	Elements
20-Stacked Tubes	942,870	5,213,424
50-Stacked Tubes	2,616,515	14,569,406
16-Stacked Tubes (less refined)	149,497	742,468
9 Tube System Heat Sink	416,397	2,391,599
64 Pin-Fin Heat Sink	385,639	1,930,144

THIS PAGE INTENTIONALLY LEFT BLANK

APPENDIX B. EXPERIMENTAL VERIFICATION.

To assess the validity of the numerical results two heat sinks were created using some of the principles uncovered during the numerical analysis. The heat sinks were designed using a square pin-fin for ease of manufacturability. A 0.25” end mill bit was used to cut the slots between the square pin-fins. or the hollow square pin-fin heat sink a drill press with a 3/16” drill bit was used to hollow out the pin-fin and additionally to provide two entrance regions into the hollowed out fin. The manufacturing of the heat sinks were lined up via eyeball vice using a computer controlled script and the vice had a little bit of play in the track system that held it to the table. Figure 22 depicts the heat sinks created for verification.

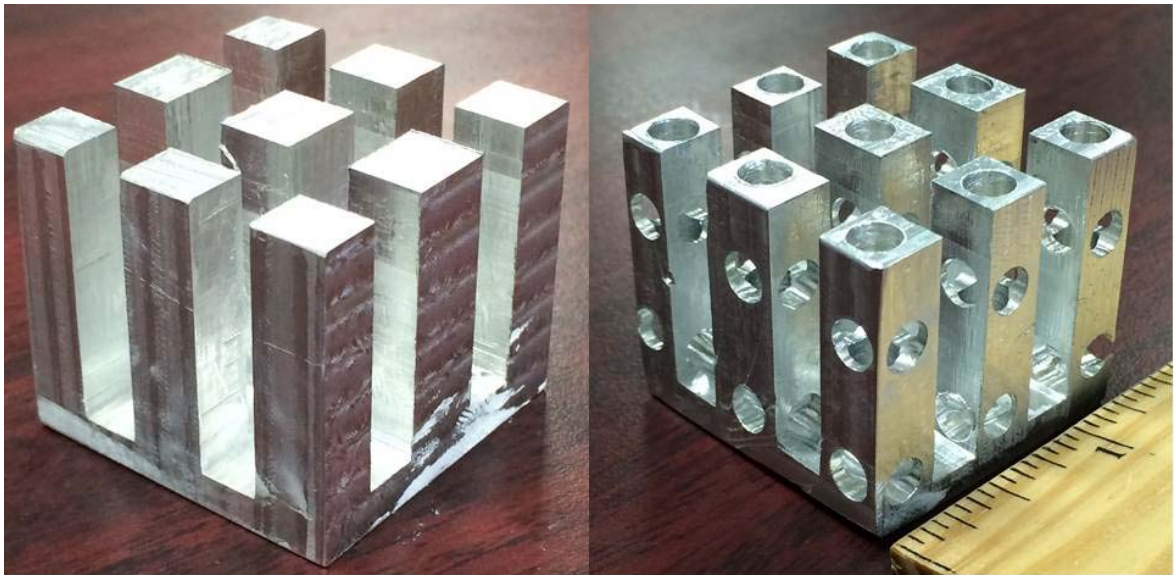

Figure 22. Heat Sinks Manufactured for Experimental Verification

The heat sinks were modeled in SOLIDWORKS accounting for imperfections created during the machining process. The heat sinks were assessed using the same numerical model used in previous analysis.

A. EXPERIMENTAL SETUP

For the experimental verification, a medical grade 1” by 1” WATLOW ceramic heater was selected as the heat source. The heater has one type K thermocouple to measure the temperature at the interface between the heater and the heat sink. Each heat sink was evaluated at four power settings ranging from 0.11 to 1.54 Watts and the temperature was recorded at each power setting once the temperature stabilized. The experiment was conducted in a lab space with an ambient air temperature of 23.0 C at the time of the experiment.

The numerical models were analyzed with both a constant temperature and constant heat flux wall boundary condition on the heat sink. The trends in both cases followed the experimental results. The constant heat flux cases were utilized for analysis since the results more closely followed the magnitude of the experimental data.

B. DISCUSSION

Figure 23 depicts the surface temperature contour with an ambient fluid streamline of the hollow square pin-fin heat sink.

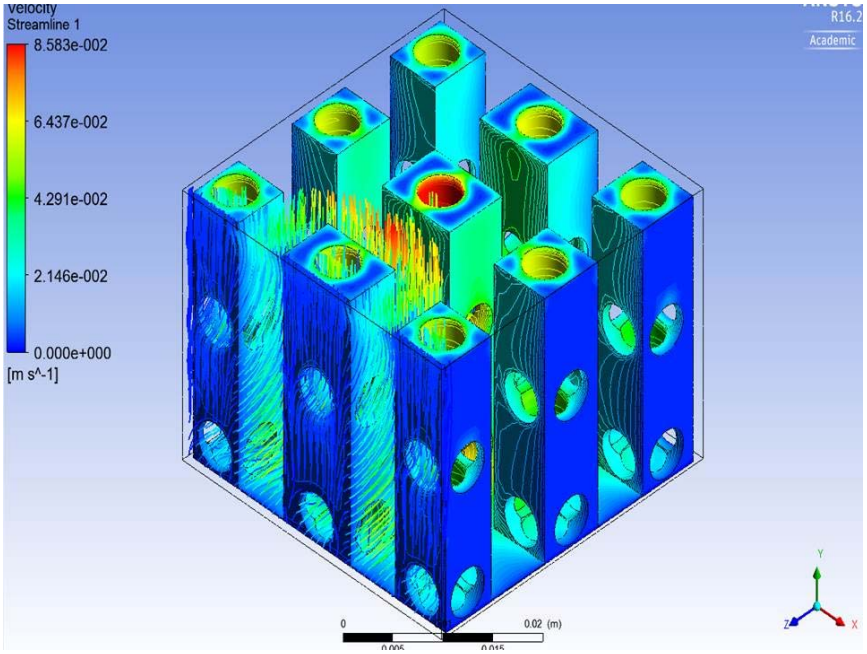

Figure 23. Hollow Square Pin-Fin Heat Sink Surface Temperature with Air Streamline Overlay

Figure 24 is a comparison of the heat flux versus temperature difference for the experimental and numerical results. This shows that the hollow square pin-fin heat sink has a lower average heat flux for a given temperature difference when compared to the solid square pin-fin heat sink. This result correlates with Awad's [11] conclusion that hollow pin-fins have the lowest heat transfer performance, based on having the lowest average heat flux.

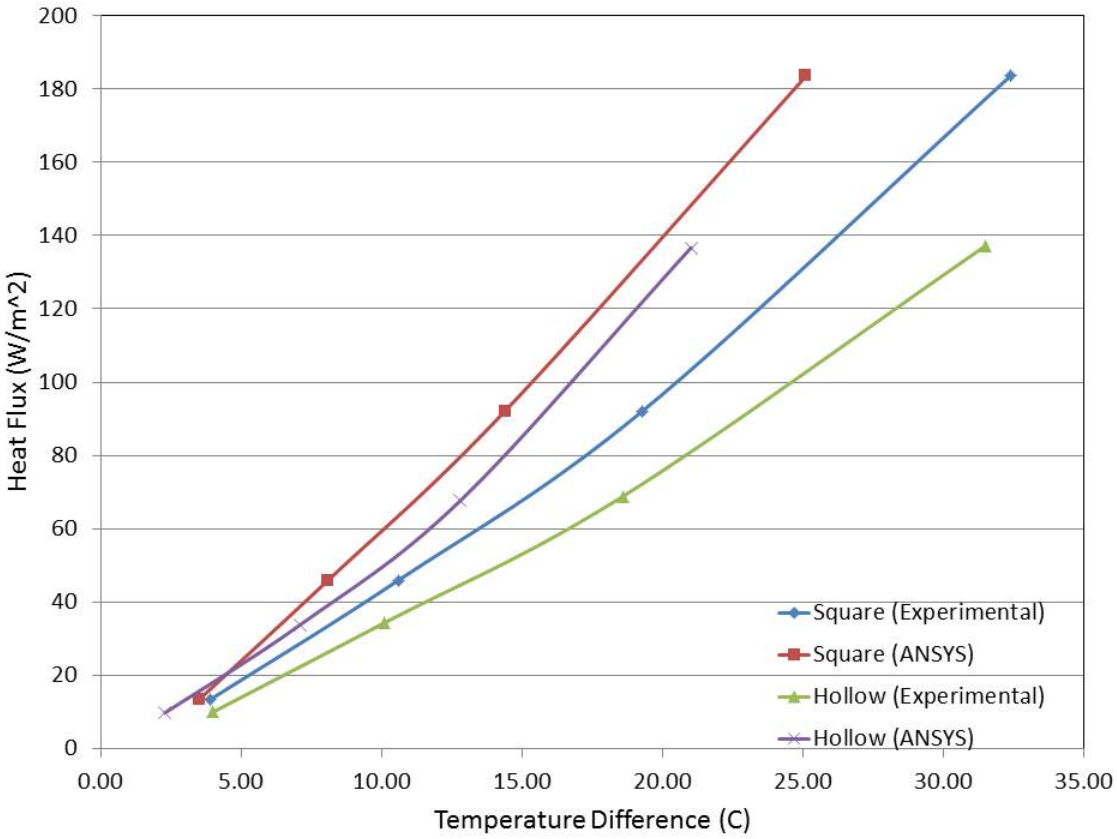

Figure 24. Comparison of Heat Flux vs. Temperature Difference

Figure 25 is plot of the temperature difference versus the power input from the heater. This figure shows that the hollow square pin-fin heat sink has a lower temperature difference for a given power input. This result correlates with Elshafei's [10] findings that hollow pin-fins have better heat transfer performance than solid pin-fins resulting from a lower temperature difference.

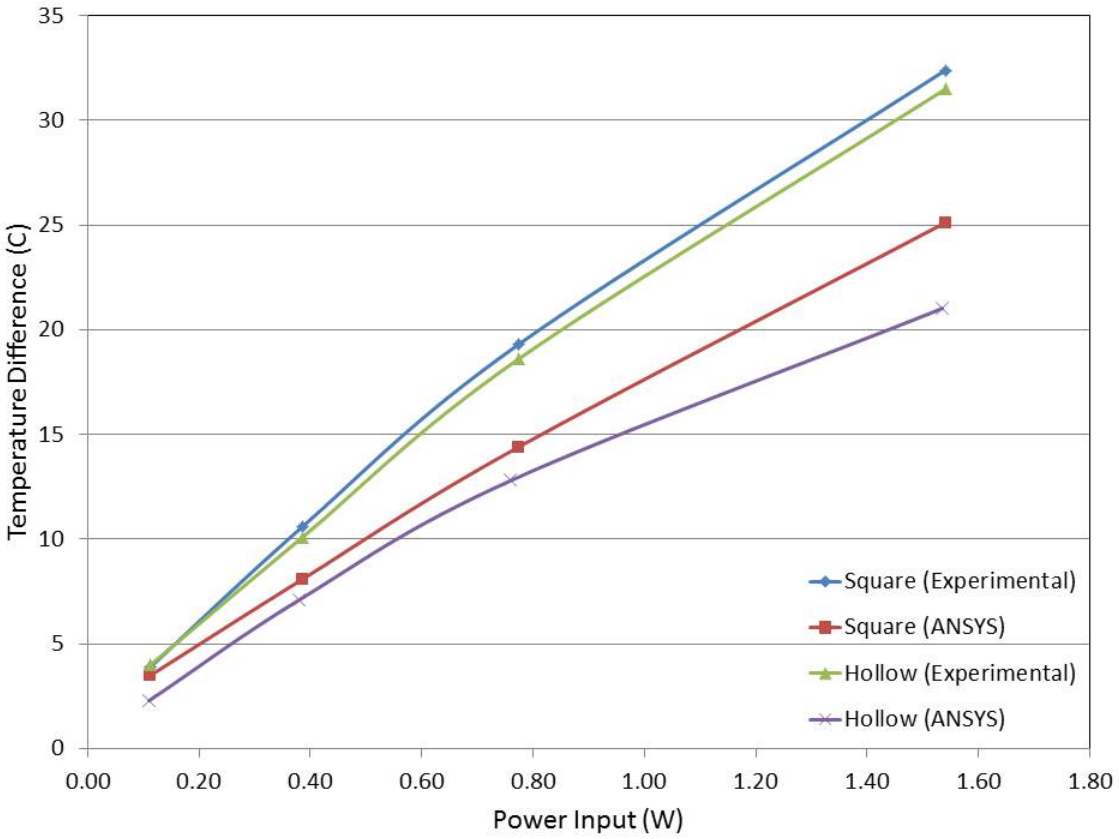

Figure 25. Comparison of Temperature Difference vs. Power Input

Based on the previous numerical results in this study one possibility to reckon the difference between Awad [11] and Elshafei [10] was based on the optimal number of hollow pin-fins in the heat sink, but Figures 24 and 25 also show that depending on how their data was plotted they could have determined different conclusions.

The average convective heat transfer coefficient is compared to the temperature difference in Figure 26. This figure shows that both experimentally and numerically the solid square pin-fin heat sink will have a higher heat transfer coefficient that the hollow square pin-fin heat sink. This result was not expected based on the previous numerical analysis conducted with circular pin-fin heat sinks.

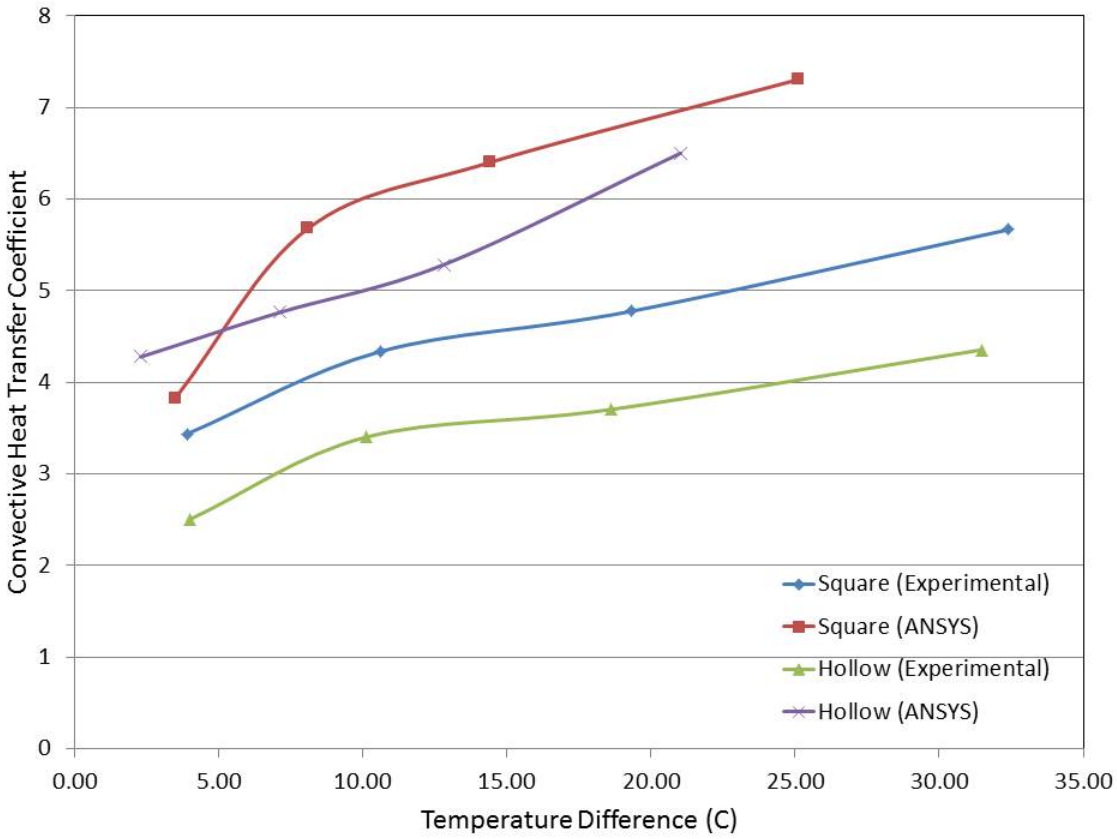

Figure 26. Comparison of Convective Heat Transfer Coefficient vs. Temperature Difference

The hollow square pin-fin heat sink does show a lower temperature difference for the same power input when compared to the solid square design, which correlates to a smaller thermal resistance as shown in Figure 27. The lower thermal resistance is due to a larger heat transfer surface area vice an increase in the heat transfer coefficient.

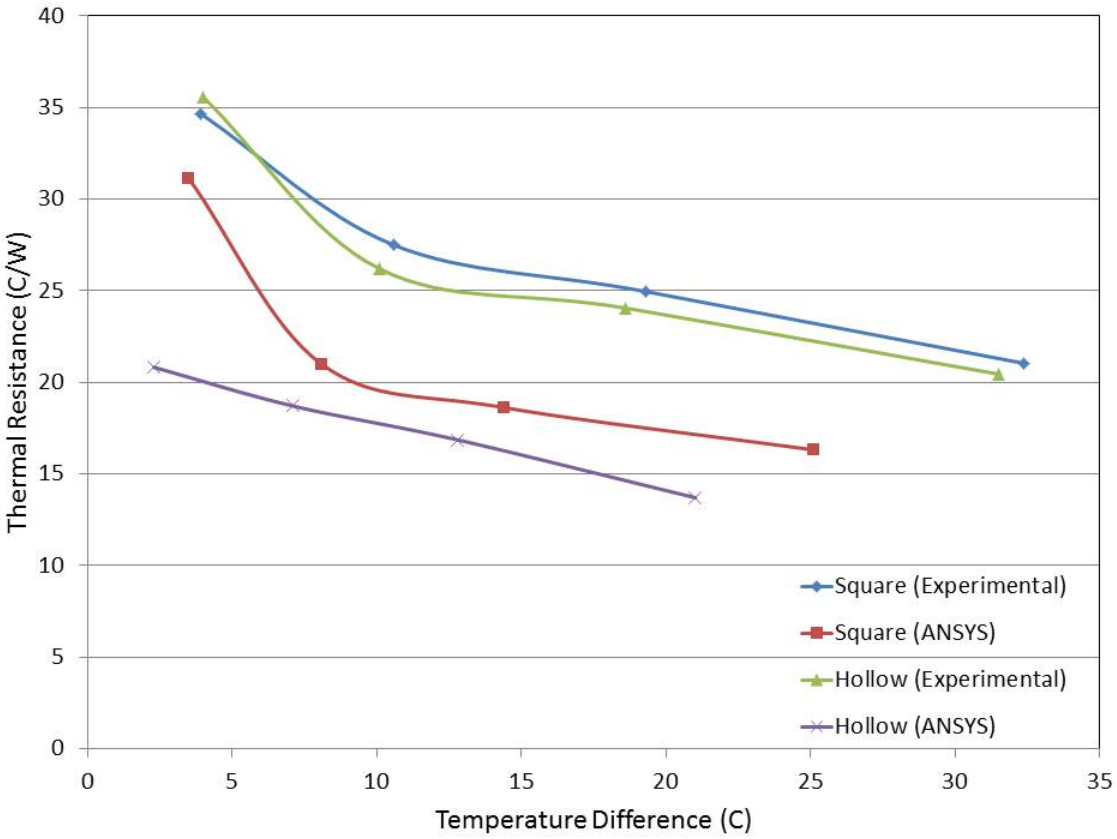

Figure 27. Comparison of Thermal Resistance vs. Temperature Difference

There are a few significant conclusions that can be drawn from this experimental validation.

- The experimental and numerical data trend together. Therefore experimentally validating the numerical model used in the previous analysis of stacked tube system heat sinks.
- Depending on how data is plotted different conclusions can be made. Therefore, it is vital to look at the results from multiple angles and assimilate all the data to make a proper conclusion.
- The hollow square pin-fin heat sink has a lower thermal resistance and uses less material than the solid heat sink. Therefore, the hollow pin-fin has better overall heat transfer characteristics than a solid pin-fin, despite having a lower average heat transfer coefficient.
- The cross-sectional profile of the fin will have a significant impact on the performance of the hollow pin-fin. The numerical study with circular hollow pin-fins shows an increase in the average heat transfer coefficient

in addition to increasing the heat transfer surface are whereas the square hollow pin-fin, both numerically and experimentally, shows a decrease in the average heat transfer coefficient when compared to its solid pin-fin counterpart.

LIST OF REFERENCES

[1] Elenbaas, W., 1942, “The Dissipation of Heat by Free Convection: The Inner Surface of Vertical Tubes of Different Shapes of Cross-Section,” Physica IX, (8), pp. 865–874.

[2] Totala, N. B., Shimpi, M. V., Shete, N. L., and Bhopate, V. S., 2013, “Natural Convection Characteristics in Vertical Cylinder,” Int. J. Eng. Sci., 3(8), pp. 27–31.

[3] Davis, L. P., and Perona, J. J., 1971, “Development of Free Convection Flow of a Gas in a Heated Vertical Open Tube,” Int. J. Heat. Mass Tran., 14(7), pp. 889–903.

[4] Sieder, E. N., and Tate, G. E., 1936, “Heat Transfer and Pressure Drop of Liquids in Tubes,” Ind. Eng. Chem., 28(1), pp.1429–1435.

[5] Incropera, F. P., Dewitt, D. P., Bergman, T. L., and Lavine, A. S., 2007, Introduction to Heat Transfer, 5th ed., Wiley & Sons, Hoboken, NJ, pp. 369–372, 482–486, chap. 6, 8.

[6] Gnielinski, V., 1976, “New Equation for Heat and Mass Transfer in Turbulent Pipe and Channel Flow,” Int. Chem. Eng., 16, pp. 359–368.

[7] Zografos, A. I., and Sunderland, J. E., 1990, “Natural Convection from Pin-fin Arrays,” Exp. Therm. Fluid. S., 3(4), pp. 440–449.

[8] Sertkay, A. A., Bilir, S., and Kargici, S., 2011, “Experimental Investigation of the Effects of Orientation Angle on Heat Transfer Performance of Pin-Finned Surfaces in Natural Convection,” Energy, 36(3), pp. 1513–1517.

[9] Huang, R. T., Sheu, W. J., and Wang, C. C., 2008, “Orientation Effect on Natural Convective Performance of Square Pin-fin Heat Sinks,” Int. J. Heat. Mass. Tran., 51(9–10), pp. 2368–2376.

[10] Elshafei, E. A. M., 2010, “Natural Convection Heat Transfer from a Heat Sink with Hollow/Perforated Circular Pin-fins,” Energy, 35, pp. 2870–2877.

[11] Awad, M. M., 2013, “Assessment of Convergent-Divergent Fins Performance in Natural Convection,” J. Am. Sci., 9(2), pp. 116–124.

[12] Krzaczek, M., Florczuk, J., and Tejchman, J., “Field Investigations of Stack Ventilation in a Residential Building with Multiple Chimneys and Tilted Window in Cold Climate,” Energ. Buildings, 103, pp. 48–61.

[13] ANSYS Fluent Theory Guide, 15th ed., ANSYS, Inc., Canonsburg, PA, 2013, pp. 625–627.

[14] Patankar, S. V., 1980, Numerical Heat Transfer and Fluid Flow, Hemisphere, New York, NY, pp. 126–130, chap. 6.

[15] Rathore, M. M., and Kapuno, Jr R. R., 2011, Engineering Heat Transfer, 2nd ed. Jones & Bartlett Learning, Sudbury, MA, pp. 589.

[16] Benedict, 2016, "Plunkett Associates uses 3D Printing to Build High Performance Heat Sinks," http://www.3ders.org/articles/20160115-plunkett-associates-uses-3d-printing-to-build-high-performance-heat-sinks.html

INITIAL DISTRIBUTION LIST

1. Defense Technical Information Center
   Ft. Belvoir, Virginia

2. Dudley Knox Library
   Naval Postgraduate School
   Monterey, California